C：岩石力學

C.1：Paper－A study on prediction of squeezing and rock burst based on surface exploration for selection of HLW disposal site in Japan

A study on prediction of squeezing and rockburst based on surface exploration for selection of HLW disposal site in Japan

K. Shin, M. Sawada & Y. Inohara
Central Research Institute of Electric Power Industry, Japan

T. Shidahara[*1], T. Hatano[*2], S. Arai[*3] & T. Miwa[*4]
*1 NEWJEC Inc., *2 J-POWER EPDC, *3 Geosphere Science Lab., *4 Tohoku Electric Power Co., Formerly at Nuclear Waste Management Organization of Japan (NUMO), Japan*

ABSTRACT: For the selection of a final repository site for disposal of vitrified high-level radioactive waste, Preliminary Investigation will be carried out in areas selected by literature survey in Japan. It is necessary to evaluate the possibility of difficulties during tunneling based on the limited data obtained in the Preliminary Investigations, which include geological explorations and geophysical and borehole surveys conducted on the surface. In this paper, criteria are proposed to predict rockburst and squeezing, based on literature surveys. More than 500 papers and construction records have been collected and analyzed. From the literature surveys, the authors have found that geological information, rock properties and stress provide good information to predict rockburst and squeezing in Japan. These findings will be effective in evaluating the construction easiness at the PI stage in which only surveys from the surface will be conducted.

1 INTRODUCTION

In Japan, the process of selection of the site for nuclear high level waste disposal is designated to be composed of three stages, namely, literature survey, Preliminary Investigations, and Detailed Investigations. Preliminary Investigations will be carried out solely from the surface. Underground characterization facility or survey tunnel will be constructed only in the stage of Detailed Investigations.

This paper is focusing on the stage of Preliminary Investigations. Based on the result of Preliminary Investigations, Detailed Investigation Area need to be selected from the viewpoints of geological stability, long-term safety and easiness of construction of the underground disposal facility. This paper deals with the viewpoint of easiness of construction, and specifically, the prediction of rockburst, squeezing, etc. which can lead to difficult tunneling. These predictions need to be based on geological and geophysical surveys on the surface and borehole survey. For the purpose of establishing the prediction methods which can be applied in the stage of Preliminary Investigations, nearly 500 tunneling reports about 280 tunnel constructions in Japan have been reviewed to extract useful information. The causes of difficult tunneling are related to (i) underground water, (ii) mechanical properties of the rock, or (iii) others such as gas. The geological factors for excessive water inflow are porous volcanic product of Quarternary, fault crush zone and hydrothermally altered zone of Green Tuff area, and degenerated mixed rock in accretionary complex. The geological factors for squeezing are solfataric clay at Quarternary volcanic zone, fault crush zone and hydrothermally altered zone of Green Tuff area, mudstone and fault crush zone of sedimentary rock of Neogene and later.

In the following chapters, rockburst and squeezing are focussed on.

2 PREDICTION OF ROCKBURST

Japanese tunnels which experienced rockbursts include Shin-Shimizu T., Dai-Shimizu T., Kan-etsu T., Karisaka T., Seihu T., and so on. Rockbursts were reported also in coal and metal mines, but those which occurred with the collapse of pillars have been excluded in this study because they are different in mechanism from rockburst in tunnels. Japanese metal mines which experienced rockbursts similar to that in tunnels include Ashio M., Ikuno M., Besshi M., and so on.

The rocks of those tunnels and mines are granite and granitic rocks, rhyolite and quartz-schist. It is said that rockburst typically occur in these kinds of blocky and hard rocks. And P-wave velocity by geophysical survey was around 5km/s at the rock of rockburst events. These information will be to some use in the geological and geophysical surveys on the surface.

2.1 *Stress and properties*

2.1.1 *Rock stress*

Rock stress data at rockburst sites have been collected to find an experimental criterion for rockburst. There are different types of stress measurement method. Firstly we used stress data measured by overcoring method because it is considered that the method is the most reliable among others.

Stress data for rockburst sites are collected from Kan-etsu T., Karisaka T., Seihu T., Kamaishi M., etc. Other stress data are also collected from underground hydropower stations where rockburst was not observed. Figure 1 shows

the distribution of σ_1 and σ_3 at rockburst sites and non-rockburst sites. ＋ and ✕ are data by other than overcoring method and not referred here. At two locations several measurements were made and they are shown by −. At another two locations stress change was measured during the advance of excavation and shown by ●. Now focusing on ● and ○, which are for rockburst occurrence and non-occurrence respectively, these two are divided in two regions in the graph fairly well. Dividing lines are drawn supposing the differential stress criterion (σ_1 - σ_3) and breakout criterion ($3\sigma_1$ - σ_3).

Since during the preliminary investigation which will be conducted only from the surface overcoring stress measurement is very difficult, stress data from hydrofracturing have also been collected to find an experimental criterion for rockburst. Figure 2 shows the distribution of σ_H and σ_h (horizontal max. and min. stress) for breakdown occurrence and non-occurrence, because breakdown and rockburst are considered similar phenomena. ● with white cross and ▲ indicate breakout for weak rock of Tertiary sediment and deteriorated rock near fault, respectively. Focusing on ● and ○ in the Figure 2, which are for breakout occurrence and non-occurrence at granitic rock respectively, these two are divided in two regions well just as in the case of overcoring stress data in Figure 1.

As shown in Figure 1 and 2, rockburst may be predictable for granitic rocks by the criteria.
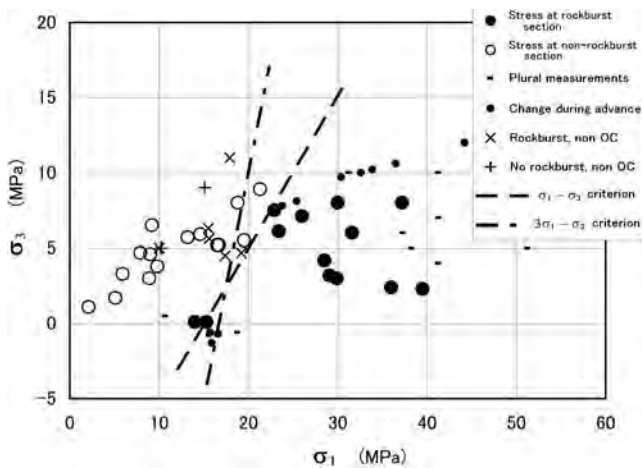

Figure 1. Rock stress (OC) and rockburst.

2.1.2 Comparison of two rocks at a site

At Kan-etsu T., hornfels appeared alternately with granite. The rock stress is hence considered almost the same for the two rock type. Rockburst, however, occurred at granite and very scarcely at hornfels. Therefore rock properties of Vp of core, Uniaxial Compression Strength (UCS), Young's modulus and poison ratio have been compared for the two rock types in Figure 3.

As seen on the graph, Vp and Young's modulus are almost in the same range of value, but UCS and poisson ratio are different. UCS of the hornfels is higher than that of the granite. This may be the reason that rockburst occurred almost only in granite. Another possible reason may be poisson ratio. The difference of poisson ratio for the two rock types is much clearer than that of UCS. Granite indicates much lower poisson ratio than the hornfels. Lower poisson ratio leads to more volumetric expansion

under the stress change during excavation and hence may lead to rockburst.

2.2 Direction of joints and rockburst

The Shin-Shimizu T., Dai-Shimizu T. and Kan-etsu T. are located within 3km from each others, and the directions of the tunnels are different by about 16 degrees consecutively. The rock is Tertiary quartz diorite and the direction of the major joint set is the same for the three tunnels. The major joint set is sub-vertical, and the angles between the tunnels' axes and the joint set are around 30, 10-20 and roughly 0 degree, respectively. Since the 3 tunnels' sites are near to each other in the same rock mass, rock stress states are also considered similar.
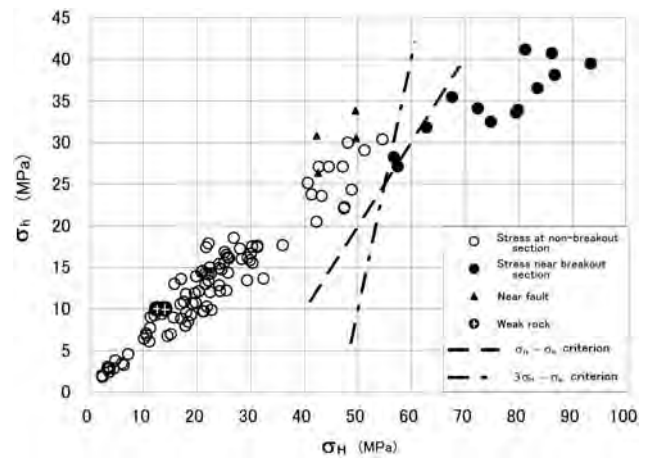

Figure 2. Rock stress (HF) and borehole breakout. σ_H and σ_h are maximum and minimum stresses in the plane vertical to the borehole. $3\sigma_H$ - σ_h is the maximum tangential stress around the borehole.
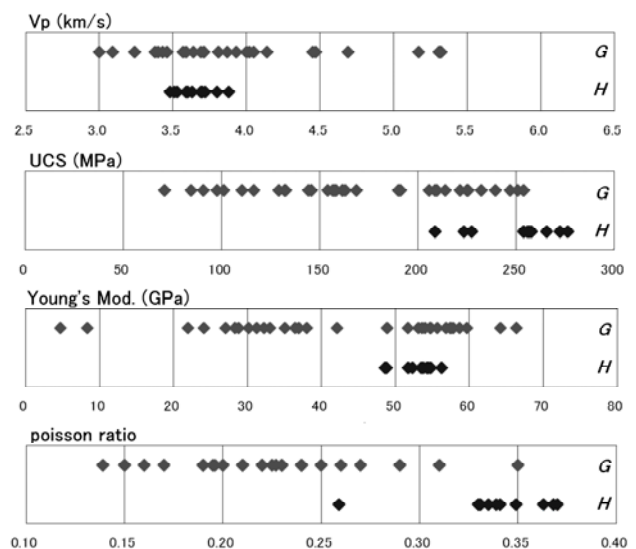

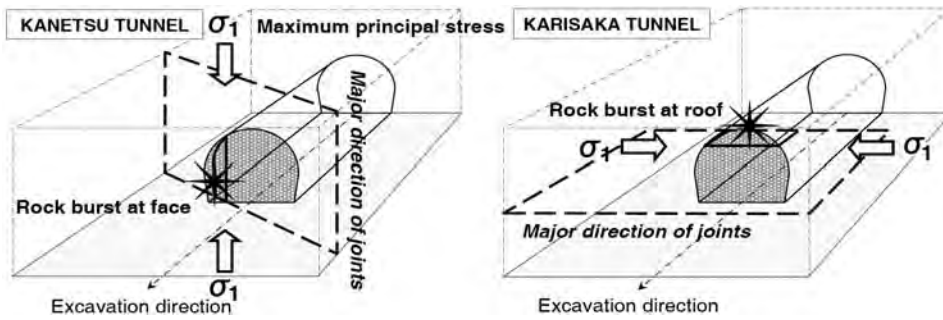Figure 3. Comparison of properties of granite and hornfels.

Figure 4. Examples of rockburst location and direction of tunnel, joint and rock stress.

The angles between the tunnel directions and the joint set show good correspondence to the location of rockburst occurrence in the tunnels.

In Kan-etsu T., rockburst often occurred at tunnel face. In Dai-Shimizu T., it often occurred around the marginal edge of tunnel face. In Shin-shimizu T., where tunnel direction is roughly parallel to the sub-vertical major joint set, rockburst often occurred at side wall.

From these examples, it is inferred that the location of rockburst event in a tunnel may be predicted from the information of relative direction of joint, tunnel and rock stress. Figure 4 shows typical examples of rockburst location and relative direction of joint, tunnel and maximum rock stress in two tunnels.

Figure 5. Relation between δ/D and UCS/σ_v .

3 PREDICTION OF SQUEEZING

Squeezing incidents of 187 have been collected from tunneling reports in Japan. About 60 tunnels among them, location of squeezing in the tunnel, the severity, geology and geological structure and rock properties could be collected. Also data of convergence δ/D was collected and used to categorize the severity of squeezing into 3 ranks of A($\delta/D<1.5\%$), B($1.5\%<\delta/D<3\%$) and C($\delta/D>3\%$). Since the squeezing is encountered mostly in soft sedimentary mudstones in Japan, the data for this type of rock is analyzed here.

As a result, it has been found that many squeezing incidents (rank C) are found near anticline, syncline and thrust fault. A few data with obvious inclination of the axis

of anticline suggest that the hanging wall has more incidents of squeezing. Also it has been found that many squeezing incidents occur in the region where Vp is less than 2.5km/s. These information will be useful in the geological and geophysical surveys on the surface.
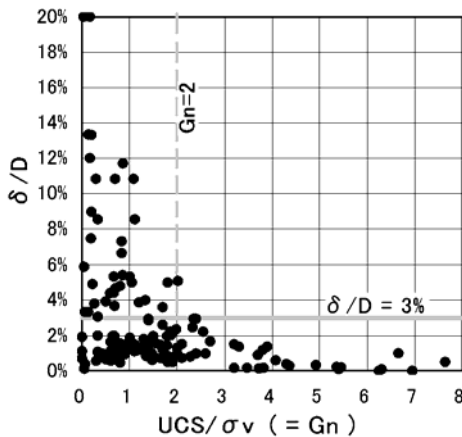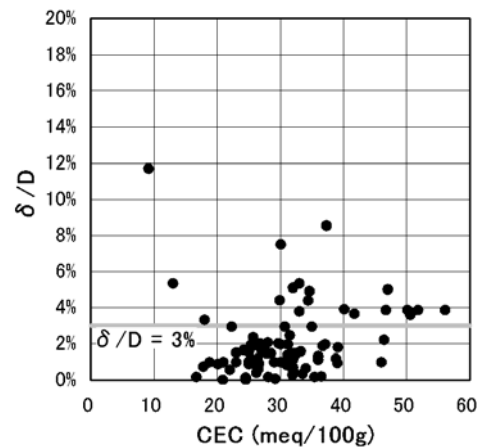

Figure 6. Relation between δ/D and CEC .

In the borehole survey, rock core will provide quantitative information about rock properties. Rock properties collected from squeezing locations include unit weight , natural water content, plasticity index, Cation Exchange Capacity, fine fraction content (under 2 μm), UCS, UCS/σ_v, sand content, etc.

Firstly, the relations between δ/D and each of the variables mentioned above have been observed. Among the variables, unit weight, UCS/σ_v, sand content, UCS and natural water content have been found to have some relations with δ/D, and other variables have not been found as such. Figure 5 is an example in the case of UCS/σ_v. Occurrence of $\delta/D>3\%$ is observed when UCS/σ_v is less than 2. Figure 6 is an example in the case of CEC. CEC is an indicator of swelling clay minerals, but collected data does not show some relations between δ/D and CEC. There are data of $\delta/D>3\%$ at a wide range of CEC.

As mentioned above, Figure 5 shows some relations between δ/D and UCS/σ_v for example, but the condition UCS/$\sigma_v < 2$ is not good enough for the prediction of squeezing of $\delta/D>3\%$ because there are many data of $\delta/D<3\%$ in the range UCS/$\sigma_v < 2$. Since squeezing is considered to be a function of multi variables, one dimensional prediction may not work well.
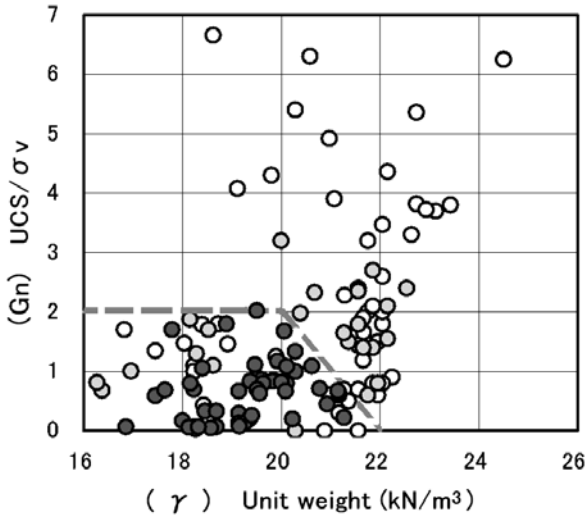
Figure 7. Distribution of 3 ranks of δ/D in the 2D-space. dark: δ/D>3%, medium: 3%>δ/D>1.5%, light: 1.5%>δ/D.
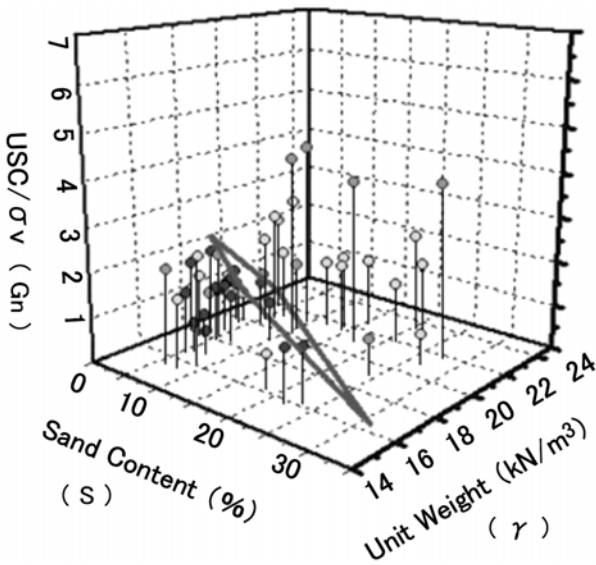

Figure 8. Distribution of 3 ranks of δ/D in the 3D-space.

Therefore the authors have tried to combine 2 parameters, UCS/σ_v and unit weight , for the better prediction of squeezing. Figure 7 shows the distribution of the data in the 2D space. Light, medium and dark grey dots indicate ranks of A(δ/D<1.5%), B(1.5%<δ/D<3%) and C(δ/D>3%), respectively. As seen on the graph, dark dots are restricted within the region bordered by grey dash lines. There are not a few exceptional data of medium and light grey dots within the region, and detailed inspection of the data have suggested that the medium and light grey dots within the region were data from sandy part of the mudstone.

Therefore the authors have tried to combine 3 parameters, adding sand content. The number of data available for the

3D analysis decreases, and Figure 8 shows the distribution of the data in the 3D space of unit weight (γ), sand content(S) and UCS/σ_v(G_n). Observing the results, the criterion for prediction of squeezing of δ/D>3% is proposed as follows.

$G_n < 2$ and

$0.0435γ + 0.00928S + 0.0765\ G_n < 1$,

where γ is unit weight (kN/m^3), S is sand content (%) and Gn is UCS/σ_v.

As depicted in Figures 7 and 8, this criterion seems to be qualitatively agreeing with common understanding.

4 CONCLUSION

For the selection of the Detailed Investigation Areas for HLW disposal, predicting the tunnel constructability (Sawada et al. 2011) is one of the requirements together with assessing long-term safety. This paper dealt with the geological factors relating to difficult tunneling such as squeezing and rockburst. Also it dealt with the prediction of rockburst and squeezing.

Information useful for predicting rockburst has been gathered from previous reports. In the Preliminary Investigation stage, geological survey, geophysical survey and borehole survey from the surface are the source of information. Therefore rock type, P-wave velocity from seismic exploration and in-situ rock stress from hydrofracturing have been considered. Majority of rockburst events occurred at granitic rock, excluding coal mine where different kind of rockburst occurred at pillars. Horizontal maximum and minimum stresses σ_H and σ_h measured by hydrofracturing have been tested as a criterion for rockburst. It has been inferred that $\sigma_H - \sigma_h$ or $3\sigma_H - \sigma_h$ criterion is a good criterion for rockburst occurrence. Continuous occurrence of borehole breakout may be a good indicator of rockburst and useful when rock stress data is not available.

This paper also dealt with the prediction of squeezing of rock in tunneling. Based on previous reports in Japan, the relationship between the degree of squeezing and geological structure, results of seismic exploration and various rock properties from laboratory tests have been analyzed for soft sedimentary rocks. It has been found that the ratio of UCS to overburden pressure, unit weight and sand content have some relations with the squeezing occurrence. Combining these 3 parameters, a criterion that may be useful for predicting the squeezing has been established.

REFERENCES

Sawada, M., Shin, K., Inohara, Y., Shidahara, T., Hatano, T. & Miwa, T. 2011. A rock mass classification to estimate excavation rate, support and rock properties in a borehole survey, ISRM 12th International Congress on Rock Mechanics, *(submitted)*

C.2：Sildes－A study on prediction of squeezing and rock burst based on surface exploration for selection of HLW disposal site in Japan

12th ISRM Congress, 2011 Oct, Beijing, China

A study on prediction of squeezing and rockburst based on surface exploration for selection of HLW disposal site in Japan.
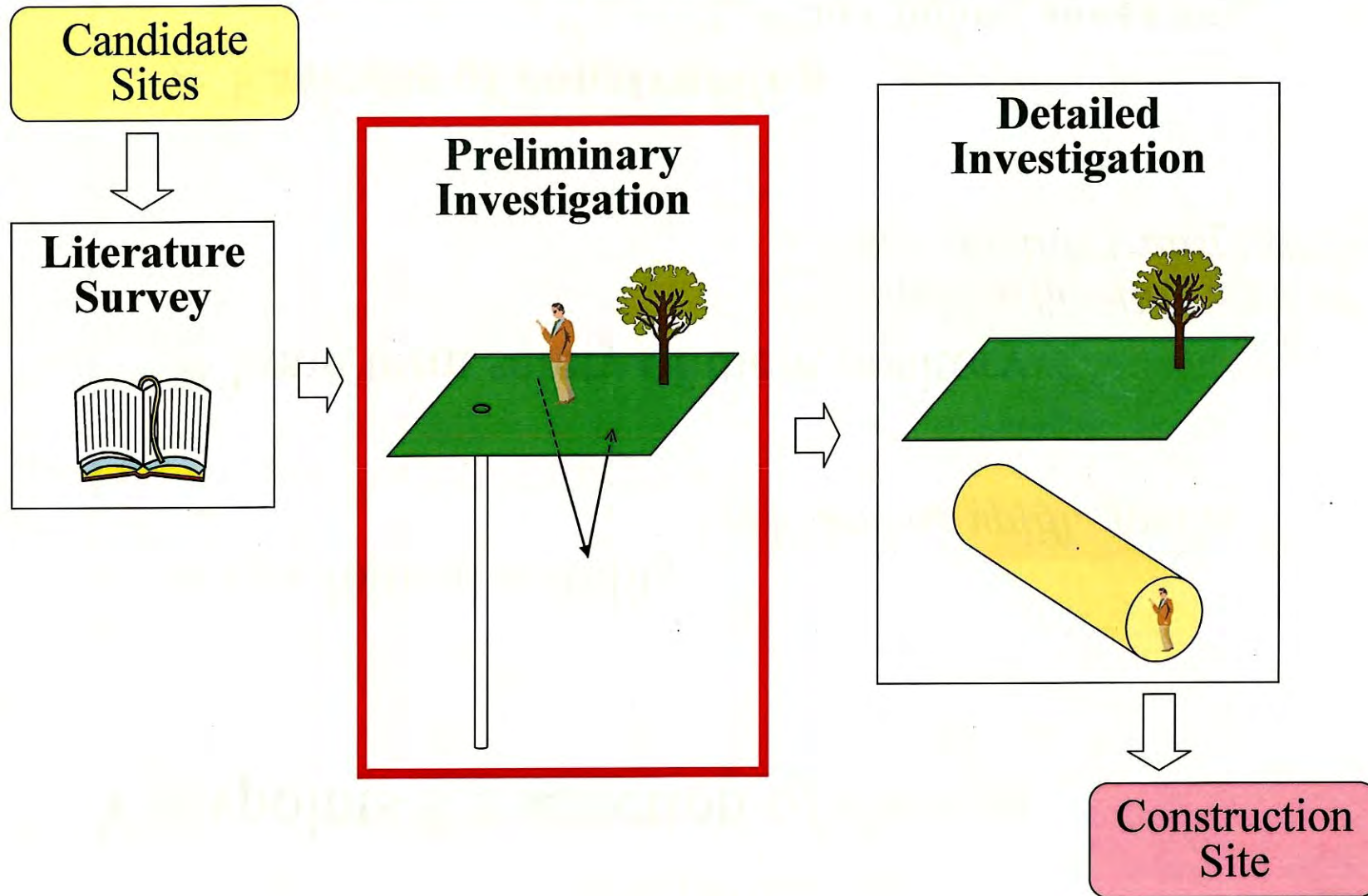
K. Shin ,

M. Sawada ,

Y. Inohara

T. Shidahara ,

H. Hatano ,

S. Arai ,

T. Miwa

Contents

1. Introduction

Selection process

Candidate Sites → **Literature Survey** → **Preliminary Investigation** → **Detailed Investigation** → **Construction Site**

1. Introduction

Viewpoints for selection of the site.

➤ Geological stability

> *Volcano, uplift, fault,,,*

➤ Long term safety of the repository

> *Barrier function against radio-nuclide transportation*

➤ **Easiness of construction** *how we have to consider.*

> *Cf. Water inflow, **squeezing, rockburst**, ,,,*

Objective of this study

As a part of assessing the easiness of construction,

procedures for rock mass evaluation specially devised **for prediction of squeezing and rockburst**,

are the **targets** to obtain.

Input for the procedure is restricted to data obtainable from the survey on the surface.
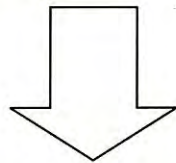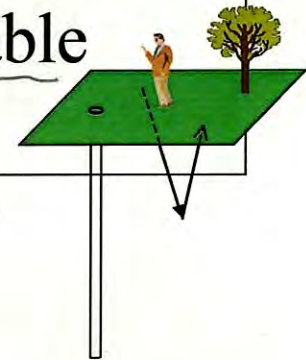
For this purpose, nearly 500 papers about 280 tunnels in Japan have been reviewed to extract useful information.

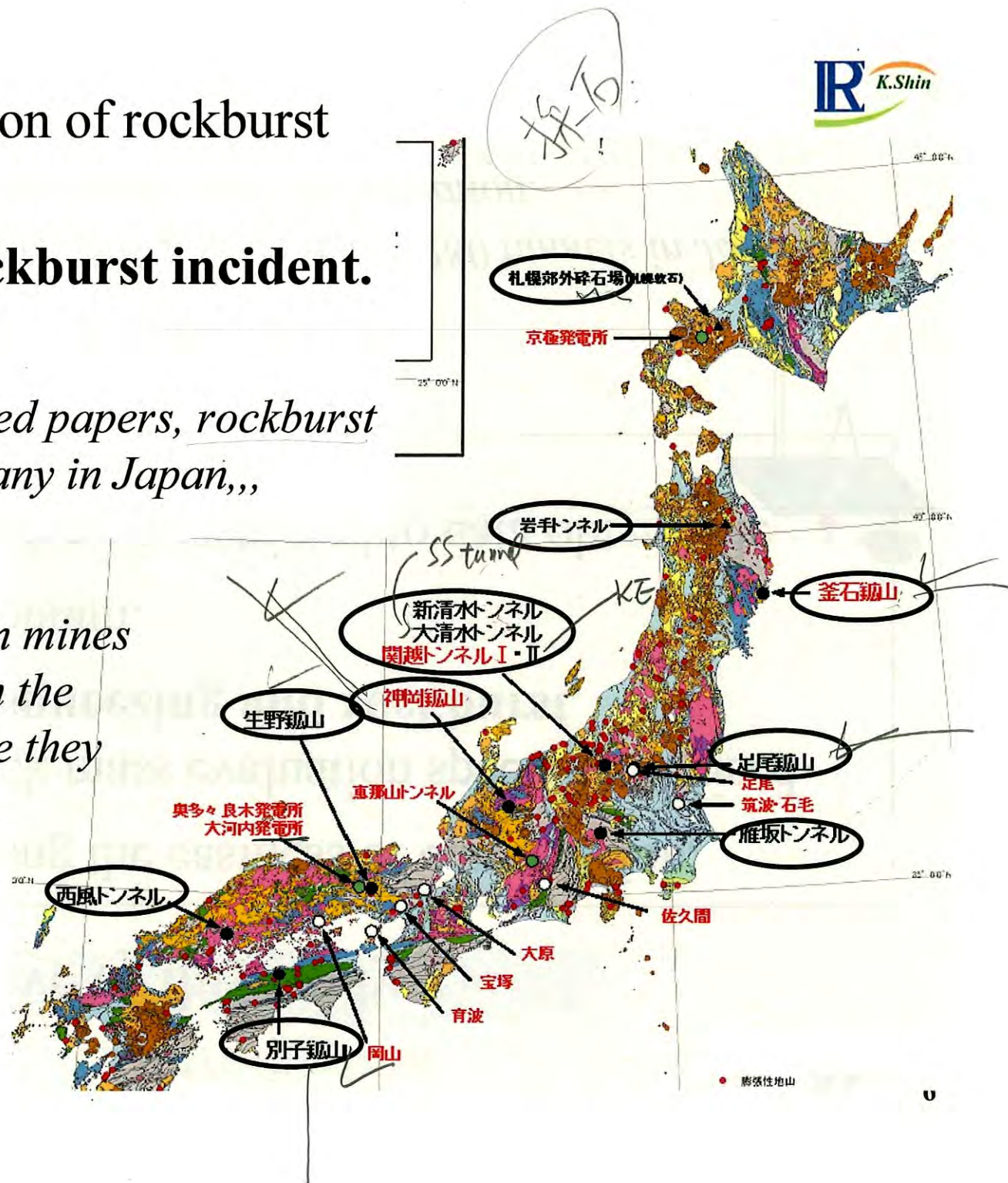# 2. Prediction of rockburst

Locations of rockburst incident.

As far as in published papers, rockburst incidents are not many in Japan,,,

Rockburst at pillars in mines have been excluded in the present study, because they may be different from rockburst at tunnels.

Description of rockburst from literatures

\<General\>

➢Most incidents occurred in granite, grano-diorite, rhyolite, tuffaceous rhyolite, and quartz schist. They are hard rocks and here they are roughly called as granitic rocks.

➢ It seems that at the rockburst section, water inflow is very limited. The rock is very tight there, concerning texture and joint.

\<SS tunnel\>

➢The phenomenon was very active within 2 hours after blasting. The activity went down with time but continued for a long time.

➢ The fragments were 2 to 30 cm in thickness and100 sq.cm to 3 sq.m.

➢ The temperature of the fragment's surface was considerably high. ←

➢ On the surface of the fragments, small spallings occurred later.

➢ After rockburst, the surface of the tunnel became very smooth in shape.
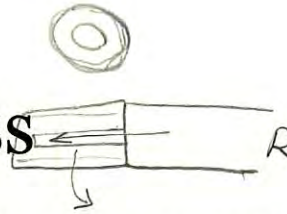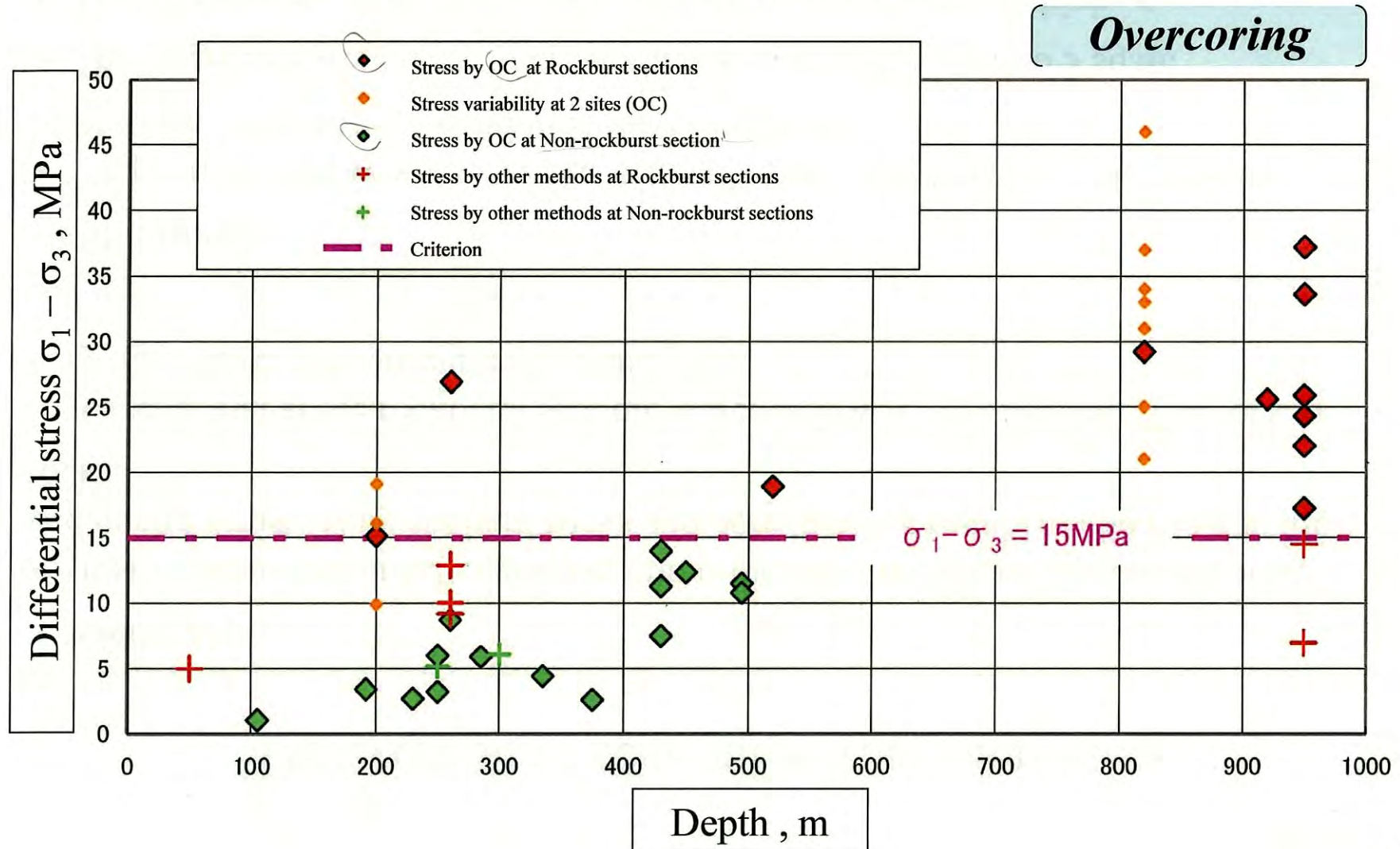
2.1.1 Rock stress

Stress data were collected to find experimental criterion for rockburst

Overcoring

Differential stress $\sigma_1 - \sigma_3$, MPa vs **Depth , m**

Legend:
- ◆ Stress by OC at Rockburst sections
- ◆ Stress variability at 2 sites (OC)
- ◆ Stress by OC at Non-rockburst section
- + Stress by other methods at Rockburst sections
- + Stress by other methods at Non-rockburst sections
- ▬ ▬ Criterion

$\sigma_1 - \sigma_3 = 15\text{MPa}$

Stress data were collected to find experimental criterion for **breakout**.
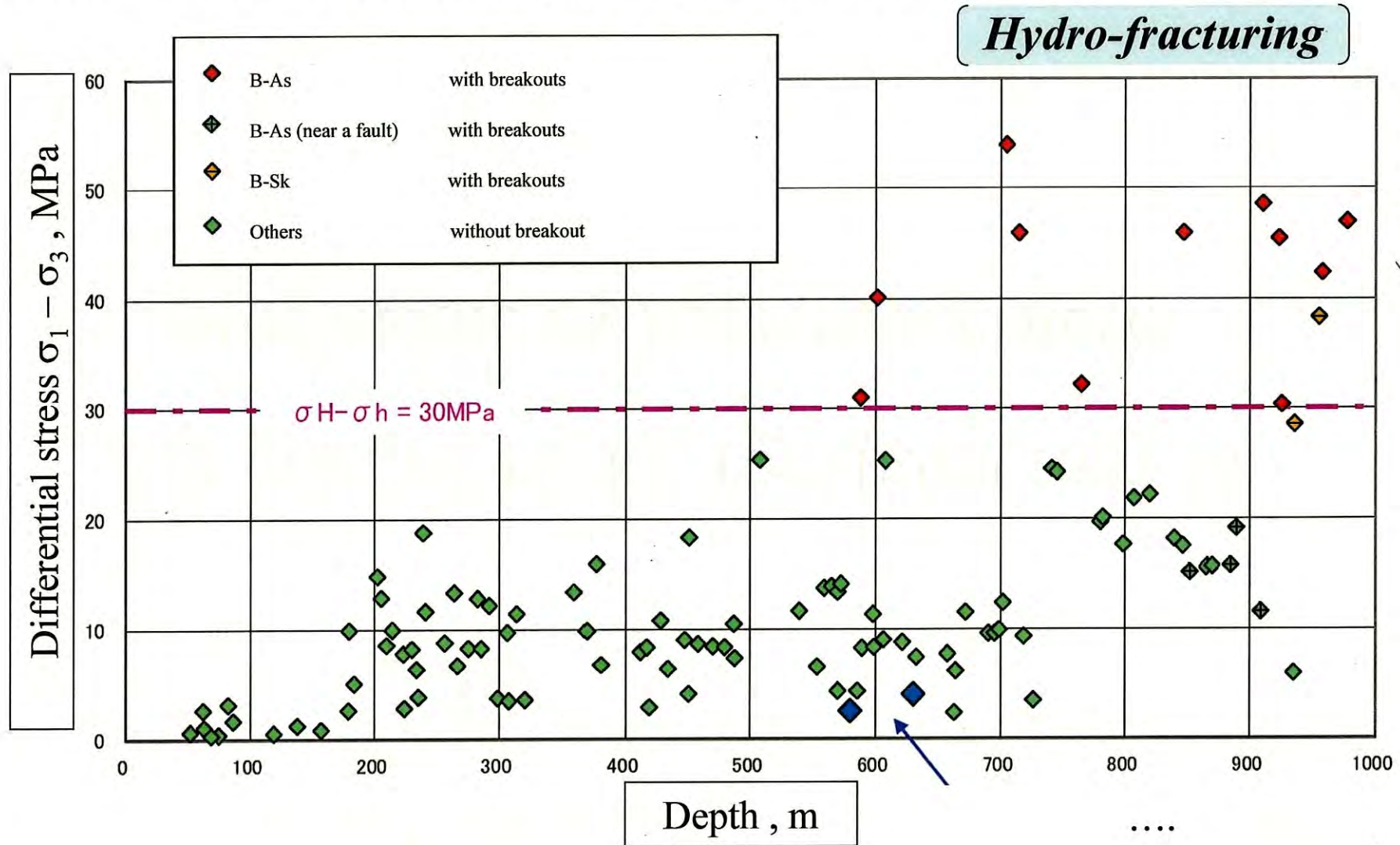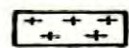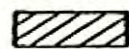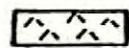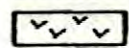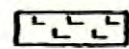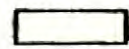
For granitic rocks, rockburst may be predictable by the stress criteria.

2.1.2 Comparison of two rocks at KE tunnel

GD and H

Gumma pref. | Niigata pref.

Mantaro shaft

Tanigawa shaft

Tf | Rh

Tf

1800
1600
1400
1200
1000
800
600
m

Rh | M | Ba | D | D | D | D

Ba

10,900 m

0 1 2 3 4 5 6 7 8 9 10 11
(km)
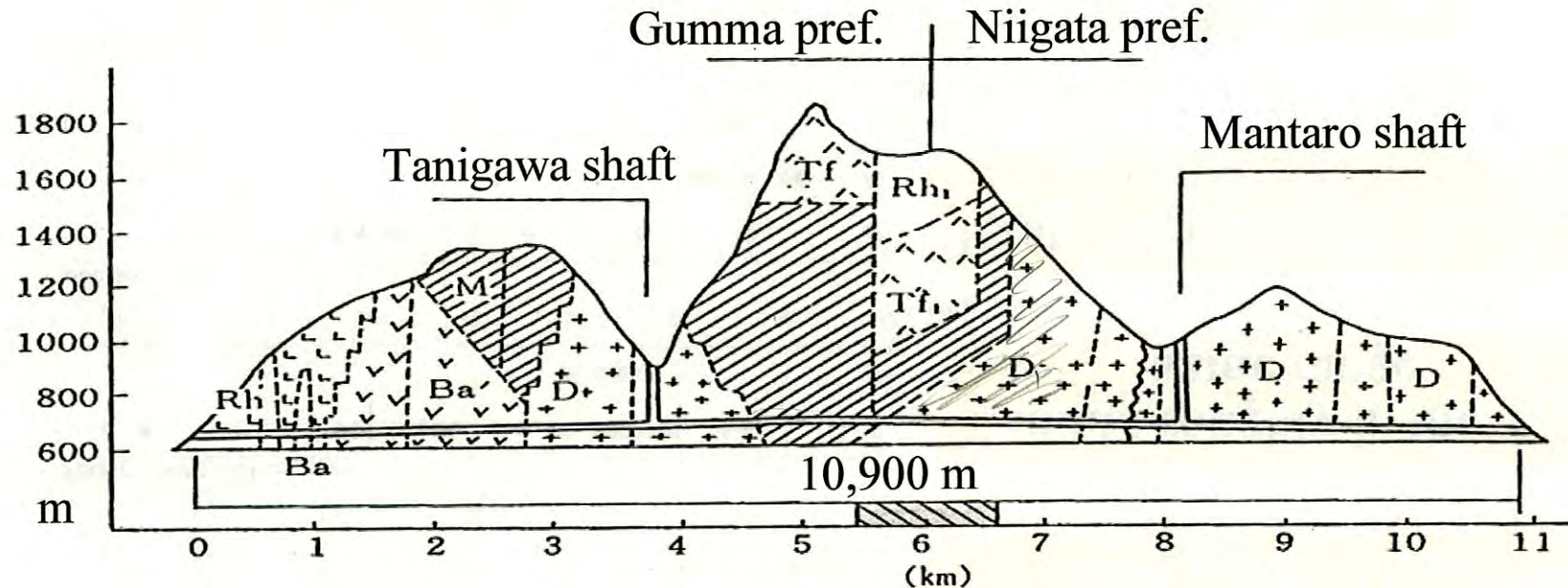
Rock burst section
Grano-diorite
Hornfels
Tuff
Basalt(degraded)
Tuffacious
rhyolite

At the KE tunnel, **rockburst occurred predominantly at granitic rock(GD), and seldom at hornfels.**

What is the difference ?

11

2.1.2 Comparison of **two rocks** at KE tunnel

GD and H

Vp (km/s) — axis: 2.5, 3.0, 3.5, 4.0, 4.5, 5.0, 5.5, 6.0, 6.5 (rows G, H)

Vp; roughly in the **same** range.   *Copress wave*

UCS (MPa) — axis: 0, 50, 100, 150, 200, 250, 300 (rows G, H)
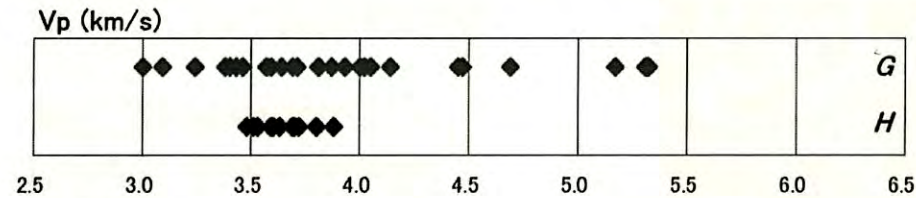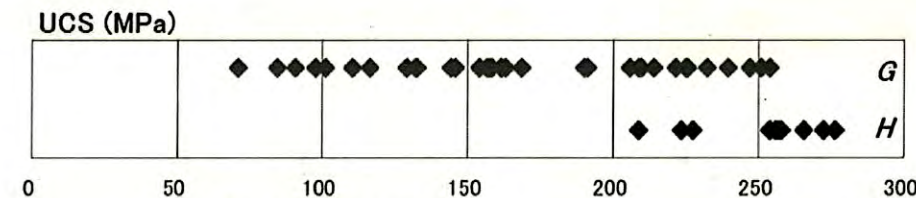
UCS; hornfels is a little stronger ★

Young's Mod. (GPa) *hard off ... Taylor* — axis: 0 *soft* 10, 20, 30, 40, 50, 60, 70, 80 *hard* (rows G, H)

Y.mod.; roughly in the **same** range.

poisson ratio — axis: 0.10, 0.15, 0.20, 0.25, 0.30, 0.35, 0.40 (rows G, H)
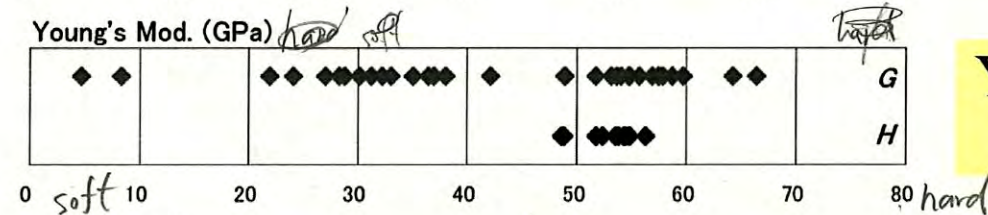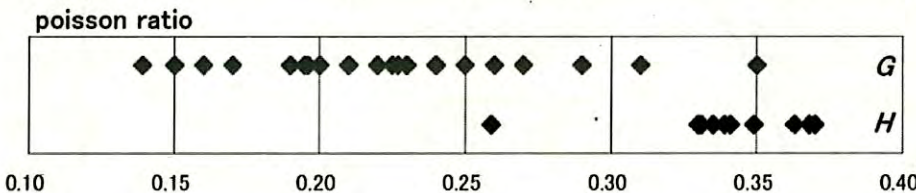
P.rat.; hornfels has higher value. ★

Volume changed   → *Volume not change*

Higher strength or higher poisson ratio may have inhibited the rockburst.

12

2.2 Direction of joints and rockburst

2.2 Direction of joints and rockburst

KE & DS TUNNEL

σ1 Maximum principal stress

direction of joints

at face

Excavation direction

KARISAKA TUNNEL

at roof

σ1

direction of joints

Excavation direction

SS TUNNEL

Maximum principal stress

σ1

direction of joints

at side wall

Excavation direction
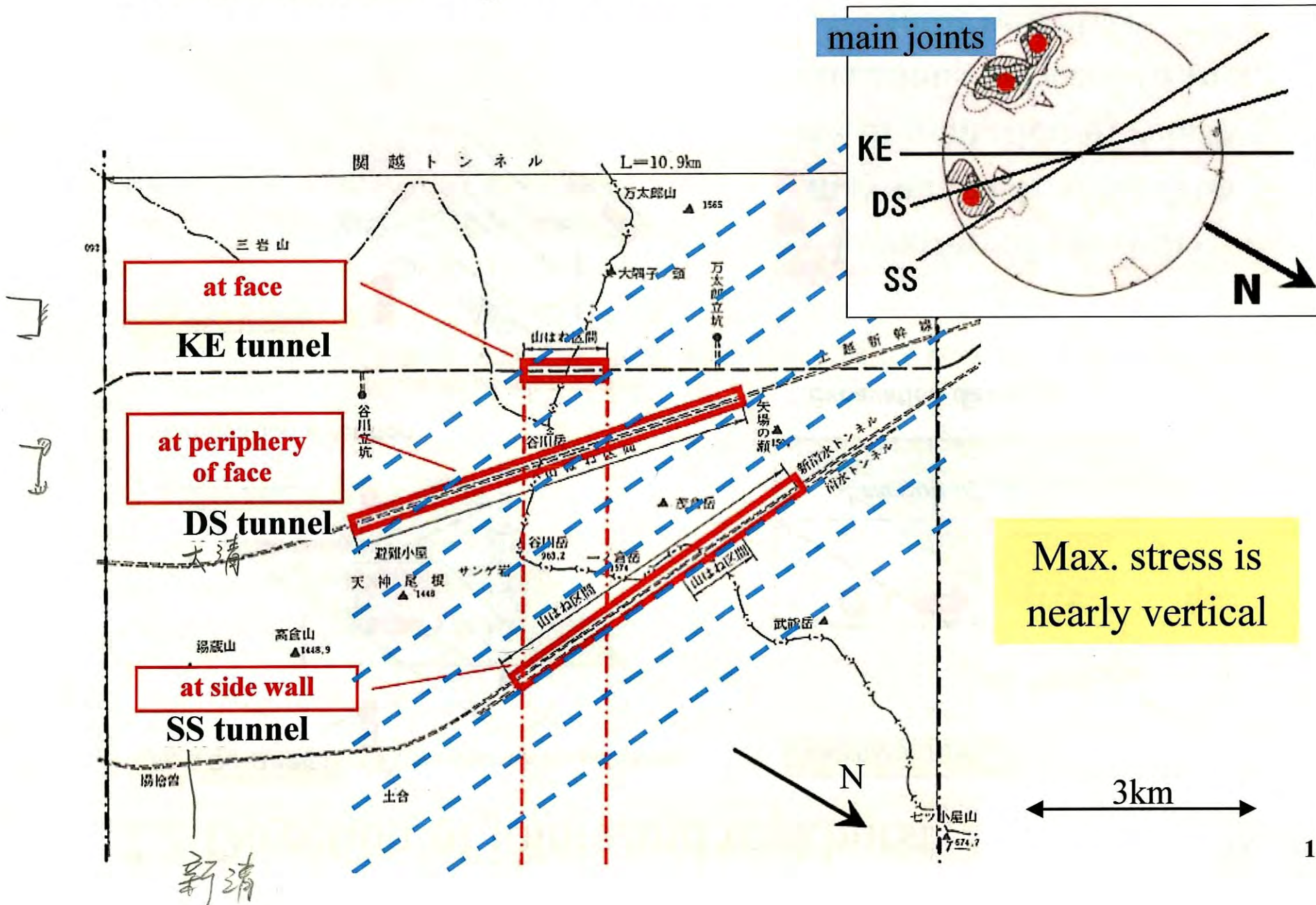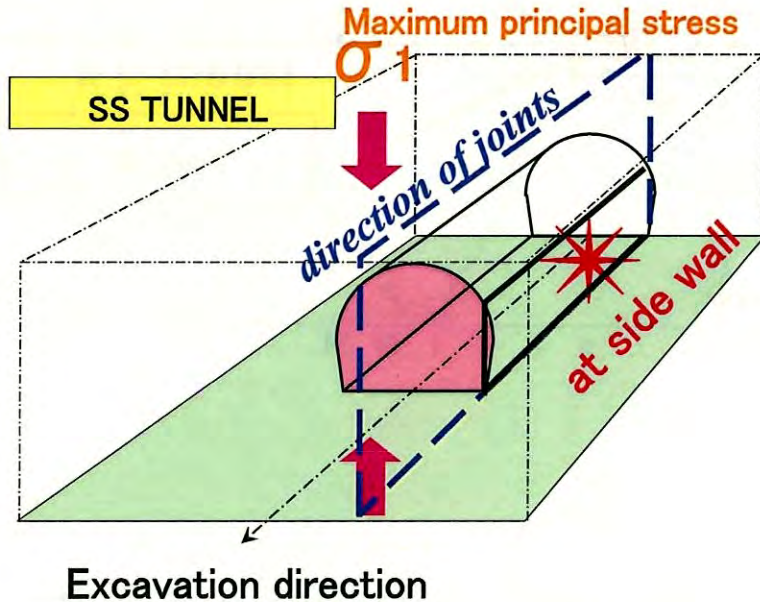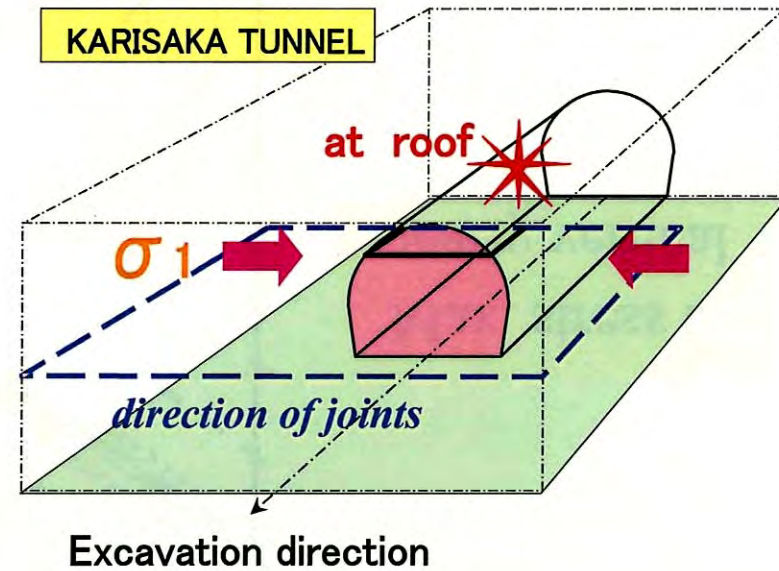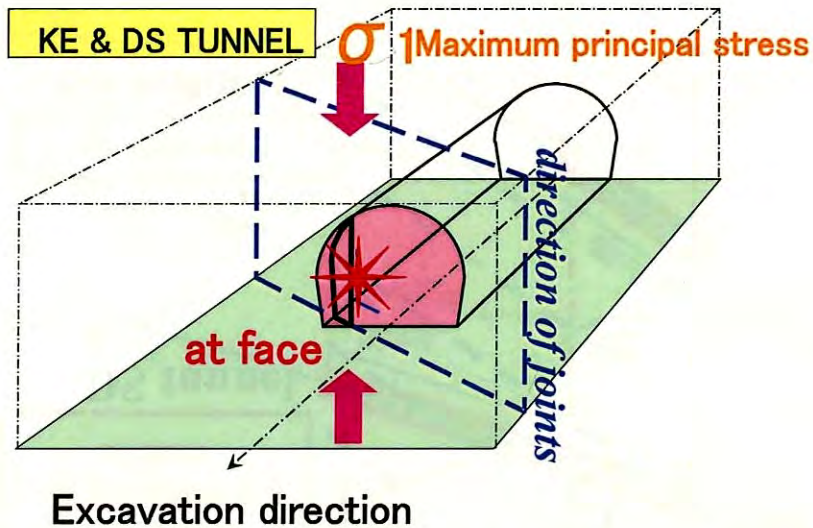
Location of rockburst may be predictable from the information of relative directions between tunnel, joint and stress.

3. Prediction of squeezing

(1) Geological Criterion

In the case of mudstone

Caution near anticline, etc

| RANK B to C |
| RANK B without C |

Horizontal distance from anticline axes (m)

TUNNEL	-2000	-1500	-1000	-500	0	500	1000	1500	2000	2500
KINDAICHI										
SHIN-ENOKI										
OHSAWAYAMA										
KASUGAYAMA										
JIZOH										
AKAKURA										
NABETACHIYAMA (CENTER)										
NABETACHIYAMA (WEST)										
NOH										
KUBIKI										
SENAMI										
IIYAMA (TOMIKURA,ARAI)										
DAIICHI-SHIRASAKA										
DAINI-SHIRASAKA										
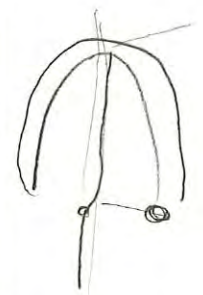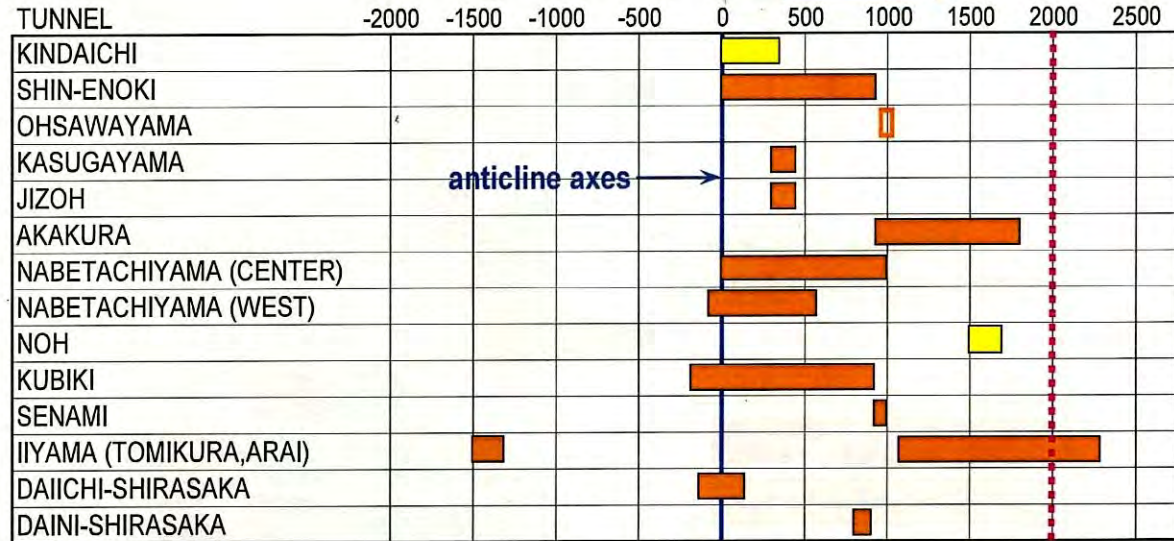
anticline axes →

Horizontal distance from thrusts (m)

TUNNEL	-2000	-1500	-1000	-500	0	500	1000	1500	2000	2500
SEIKAN (SAYOSHI)										
IIYAMA (KONARI,ITAKURA)										

thrusts →

2000m
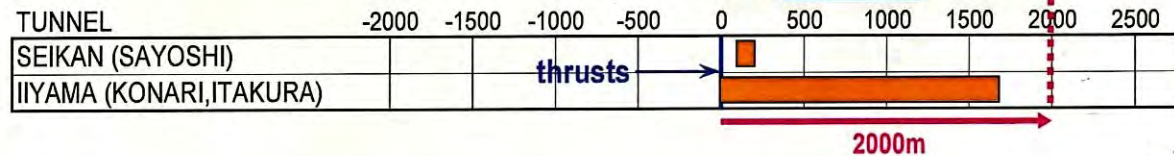
Horizontal distance from syncline axes (m)

TUNNEL	-2000	-1500	-1000	-500	0	500	1000	1500	2000	2500
SEIKAN (CENTRAL SEA)										
IIYAMA (HIGASHI-SUGANUMA)										

syncline axes →

500m
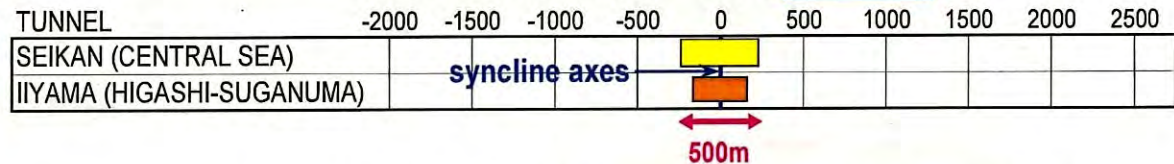
Vertical distance below surfaces of unconformity

TUNNEL	0	50	100	150	200	250	300
NICREYAMA							
HORIKOSHI-DAINI							
ENREI							

surfaces of unconformity →

100m
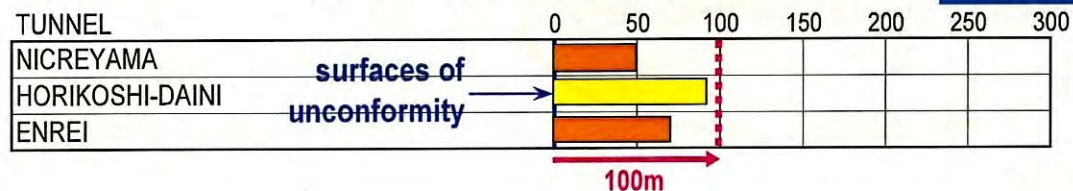
3. Prediction of squeezing

(2) Geophysical Criterion

Caution when Vp is low

In the case of mudstone

TUNNEL	Seismic ground velocity (Vp;km/s)
SEIKAN (CENTRAL SEA AREA)	← inside tunnel
NICREYAMA	
JIZOH	
NOH	
NABETACHIYAMA (CENTER - EAST)	
NABETACHIYAMA (WEST)	
SENAMI	
IIYAMA (TOMIKURA)	
IIYAMA (KONARI)	by high resolution seismic refraction method
IIYAMA (ITAKURA)	
ENREI	
DAIICHI-SHIRASAKA	
DAINI-SHIRASAKA	

INDEX

δmax/D < 1.5%	A
1.5% ≤ δmax/D < 3%	B
3% ≤ δmax/D < 5~6%	C
5~6% ≤ δmax/D	

16

(3) Geomechanical Criterion

In the case of mudstone

Almost all the incidents of more than 3% squeezing are in the region Gn < 2.

Gn < 2

Necessary condition but not sufficient.

17
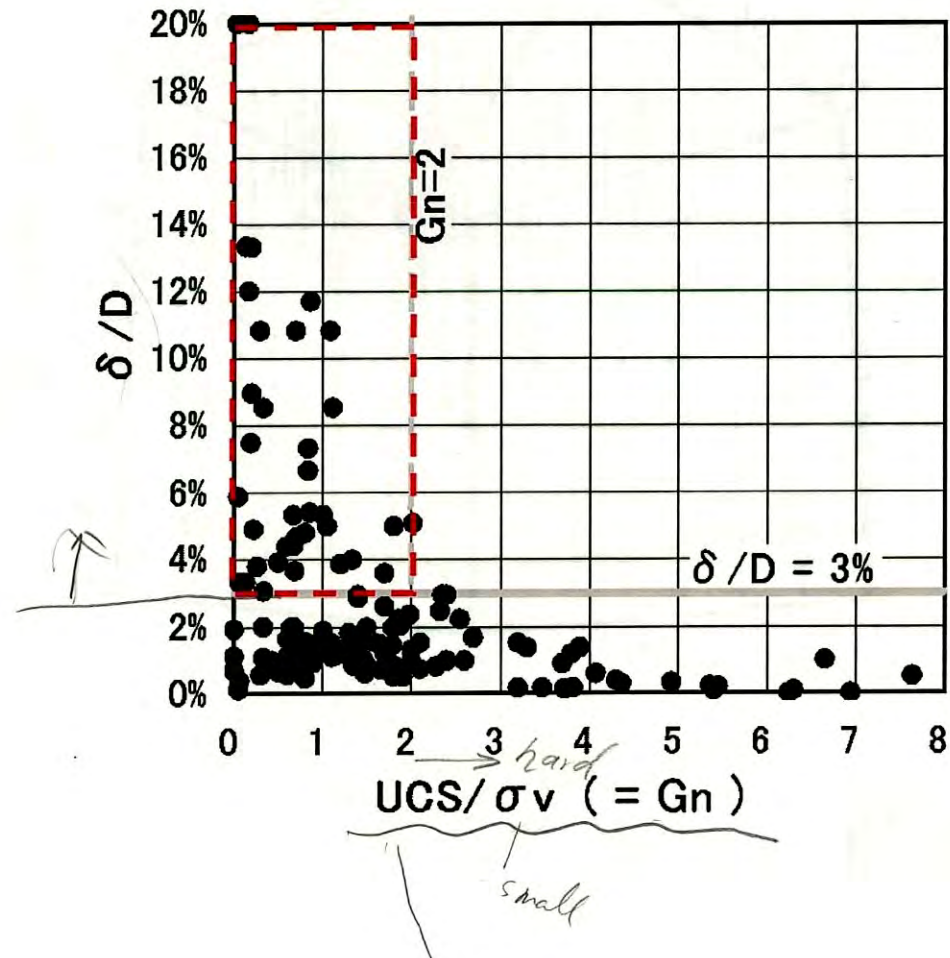
3. Prediction of squeezing

(3) Geomechanical Criterion

In the case of mudstone

3 parameters criterion

γ : unit weight (kN/m³),

S : sand content (%),

G_n : UCS/σ_v.
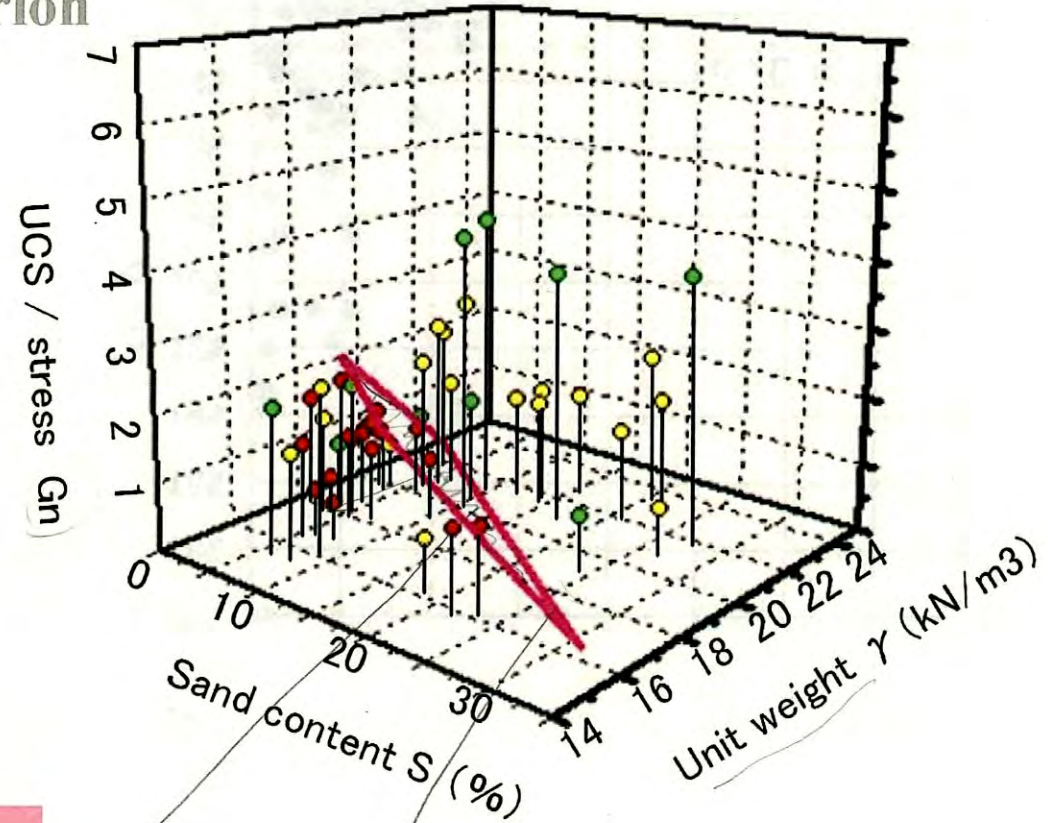
Gn < 2　　and

$0.0435\gamma + 0.00928S + 0.0765 G_n \leqslant 1$

- 🟢 : δ max/D < 1.5%
- 🟡 : 1.5% < δ max/D < 3%
- 🔴 : 3% < δ max/D and heavy support

18

4. Conclusion

For the purpose of predicting the **squeezing and rock burst**, Japanese tunneling literatures have been surveyed and analyzed.

Some affecting factors have been found that will be useful to use in the Preliminary Investigation Stage for selecting the final disposal site of nuclear waste.

	Geological	Geophysical	Geo-mechanical
Squeezing	anticline, syncline, ,,	small Vp	S-γ-Gn
Rock-burst	granitic	high Vp	in-situ stress (joint directions)

The end

C.3：Paper－Predictive analysis of tunneling difficulty

Predictive analysis of tunnelling difficulty

Takumi Shidahara, Koichi Shin, Masataka Sawada & Yoshiki Inohara
Central Research Institute of Electric Power Industry, Abiko City, Japan

Toru Arai
Geosphere Science Laboratory,Tokyo, Japan

Makoto Asakawa
Nuclear Waste Management Organization of Japan, Tokyo, Japan

SYNOPSIS: For the selection of a final repository site for disposal of vitrified high-level radioactive waste, preliminary investigations will be carried out in areas selected by literature survey. It is necessary to evaluate the possibility of difficulties during tunneling based on the limited data obtained in the preliminary investigations, which include geological explorations and geophysical and borehole surveys. In this paper, evaluation criteria are proposed as indicators for the occurrence of difficulties during tunneling, such as squeezing ground and rock burst, based on existing literature information on tunneling difficulty. In the case of squeezing ground, difficulties arise when the tunnel strain (displacement / tunnel diameter) is larger than 3% or when tunneling requires replacement of timbering or selection of a circular cross-section to prevent further internal displacement. Evaluation criteria are proposed for the prediction of squeezing ground based on geological structure, elastic wave velocity and the results of laboratory tests using core specimen. In the case of rock burst, evaluation criteria are also proposed based on rock type, elastic velocity and data obtained by borehole surveys, including in-situ stress, rock properties and the orientation of joint systems.

1. INTRODUCTION

The Specified Radioactive Waste Final Disposal Act defines a three-stage site selection process, which proceeds from literature studies to selection of preliminary investigation areas (PIAs), in which surface-based investigations will provide the basis for selection of detailed investigation areas (DIAs). Detailed investigations will include the construction of underground characterization facilities and will then lead to the selection of a final repository site (Figure 1). Ease of construction of the repository is an important indicator for the suitability of a repository site and will be evaluated in stepwise investigations. Rock properties therefore require to be evaluated appropriately and difficulties with tunneling should be avoided as far as possible. Particularly in the selection of detailed investigation
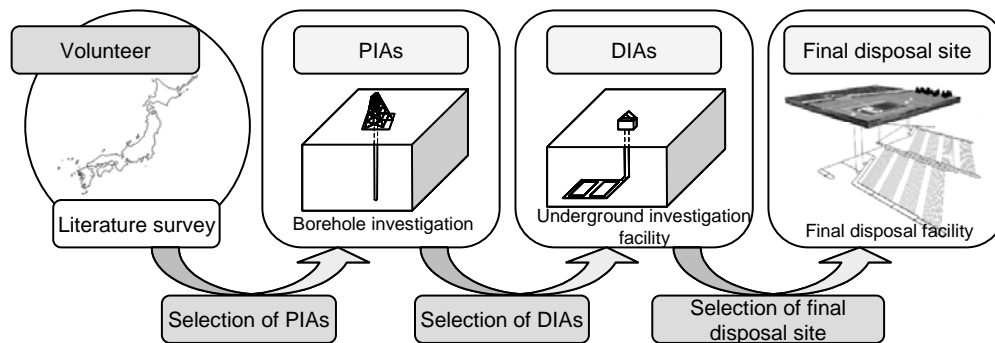

Figure 1 Three-stage site selection process for the final disposal of radioactive waste

areas, it is necessary to make important decisions leading to procurement of land and construction of an underground laboratory based on the limited data obtained in the preliminary investigations, i.e. surface-based investigations such as trenching, geophysical investigations and borehole surveys. Therefore, it is important to establish advanced methods for evaluating rock properties and for predicting tunneling difficulties based on the limited data obtained in the preliminary investigations.

Evaluation criteria in the preliminary investigation stage are proposed (Shidahara et al., 2007[1]) as indicators related to the occurrence of difficulties with tunneling, such as squeezing ground and rock burst, based on information from previous relevant tunneling projects. Regarding squeezing ground, which is defined as tunnel displacement divided by diameter ($\delta max/D$) $\geq$ 3% (Kojima at al., 1989[2]), criteria for predicting the occurrence of tunneling difficulties were proposed based on geological structure, elastic wave velocity and the results of laboratory tests. This evaluation method has been applied in the past to tunnels deep underground in mudstone. With regard to rock burst, an evaluation method is proposed based on in-situ stress, rock properties and the orientation of rock joints, derived from analyses of previous tunnel construction projects that included occurrences of rock burst. This evaluation method has also been applied in the past to tunnel construction deep in granitic rock. The proposed evaluation criteria, the methods and their application are reported below.

2. EVALUATING EASE OF CONSTRUCTION

2.1 Complex geological setting of Japan and evaluation of rock properties

In order to evaluate the suitability of candidate sites for the final repository, it is necessary to predict rock properties and the difficulty of constructing disposal tunnels that will be located more than 300 m below ground surface. Generally speaking, evaluation of rock properties deep underground is difficult, particularly in the preliminary investigation stage which includes only a limited number of borehole surveys. Japan is located in a tectonically active zone at the edge of the Eurasian continent and its rock faces are very complex. As shown in Figure 2, difficulties with tunneling relate to geological age and rock type. Squeezing ground occurs mainly in mudstone but also in other rock types.

2.2 Evaluation of rock properties from the viewpoint of ease of construction

For the evaluation of rock properties in the construction of mountain tunnels and underground fuel storage tanks, investigations in pilot and main tunnels are very important in addition to surface-based investigations such as geophysical investigations and borehole surveys. However, in the preliminary investigation stage, investigation measures will be limited and effective surface-based investigation methods are required for evaluating rock properties and predicting tunneling difficulty.

Figure 2 Geological classification for tunnelling difficulty in Japan: examples of squeezing ground and rock burst

As shown in Figure 3, a new approach for evaluation of rock properties consisting of a method for rock classification by scoring and predictive evaluation of tunneling difficulty has been proposed. Using the method for rock classification by scoring, physical properties and ease of construction (including tunneling rate and specification of tunnel support) can be evaluated. Using predictive evaluation of tunneling difficulty, the likelihood of occurrence of squeezing ground and rock burst will be assessed, allowing suitability as a candidate site for a repository to be evaluated.

In this report, the focus is on prediction of tunneling difficulty rather than on the method for rock classification by scoring.

3. PREDICTION OF SQUEEZING GROUND

3.1 *Procedure for the prediction*

As shown in Figure 2, squeezing ground occurs in various rock types. In this paper, the procedure and evaluation criteria for the case of mudstone are discussed because there are many precedents for squeezing ground in mudstone. Tunneling difficulty in squeezing ground is defined as a tunnel with strain (displacement / tunnel diameter ($\delta max/D$) $\geq$ 3%, corresponding to rank C in Table 1. Tunnels

requiring the replacement of timbering and selection of circular cross-sections are also included in difficult tunneling. The evaluation procedure consists of a surface exploration stage, a geophysical investigation stage and borehole survey stage (Figure 4). At each stage, the evaluation of rock properties deep underground will be revised in accordance with the accuracy of the investigations and borehole surveys will be focused in areas judged to be hazardous in previous stages.

3.2 *Predictive evaluation criteria for each stage*

Predictive evaluation criteria for each investigation stage are developed from indicators obtained from data on past examples of difficult tunneling. In the case of mudstone, evaluation criteria in the surface exploration stage are derived from geological structure. As shown in Figure 5, the probability of tunneling difficulty due to squeezing ground will be high if the tunnel is located within 2 km of an anticline axis or a thrust. If the target area has evidence of landslides, particular attention will also be necessary. In most cases of difficult tunneling, the elastic wave velocity is lower than 2.5 km/s, as shown in Figure 6a, and this is therefore taken as the evaluation criterion for the geophysical investigation stage.
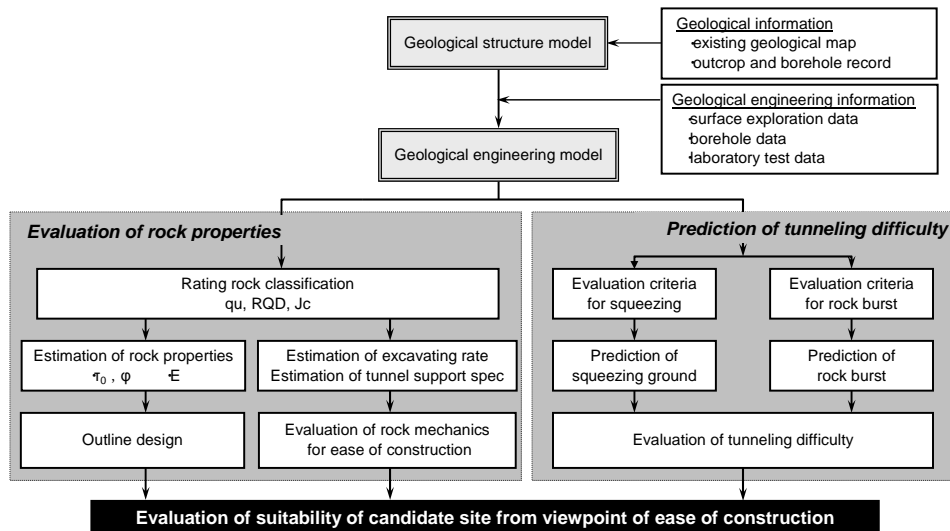
Figure 3 Flow diagram of rock quality evaluation for tunnelling in the preliminary investigation stage

Table 1   Criteria for difficult tunnelling in squeezing ground

RANK		Strain of tunnnel wall (methods)
DIFFICULTY RANK	A	δmax/D < 1.5%
	B	1.5 ≤ δmax/D < 3%
	C	3% ≤ δmax/D (replacing of timbering) (circular cross-section)

Geological exploration stage	Geophysical investigation stage	Borehole survey stage
Literature survey / **Field survey**	**Positioning for seismic survey**	**Positioning for drilling**
CRITERIA FOR GEOLOGICAL STRUCTURE / *within 2km of anticline axes or thrusts*	**CRITERION FOR SEISMIC VELOCITY** / *Vp ≤ 2.5km/s*	**Depth-dependent state of physical properties**
		Distribution of physical properties
Estimation of ground plasticity by landslide investigation	**Estimation of deep structure**	**CRITERIA FOR PHYSICAL PROPERTIES** / *Gn < 2 & 0.0435γ+0.00928S+0.0765Gn ≤ 1* / Gn:competence factor,γ:unit weight, S:sand content
		Spatial estimation of squeezing ground

Figure 4 Evaluation stages and flow diagram for prediction of squeezing ground in the case of mudstone

Figure 5
Criterion 1 for the case of mudstone geological characteristics

Figure 6
Criterion 2 for the case of mudstone – elastic wave velocity

At the borehole survey stage, laboratory tests are carried out to predict tunneling difficulty in areas judged in previous stages to be likely to show tunneling difficulty. Evaluation criteria consist of the competence factor (Gn), unit weight (γ)and sand content (S) as shown below.

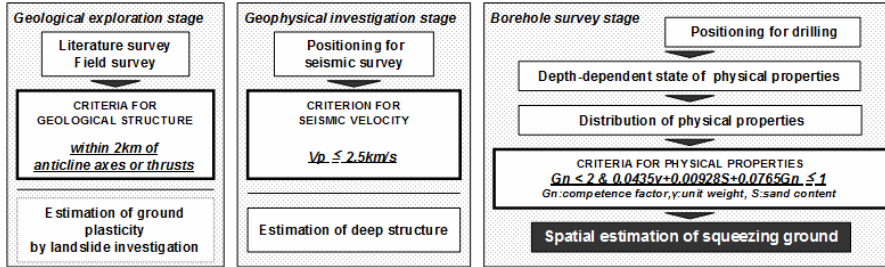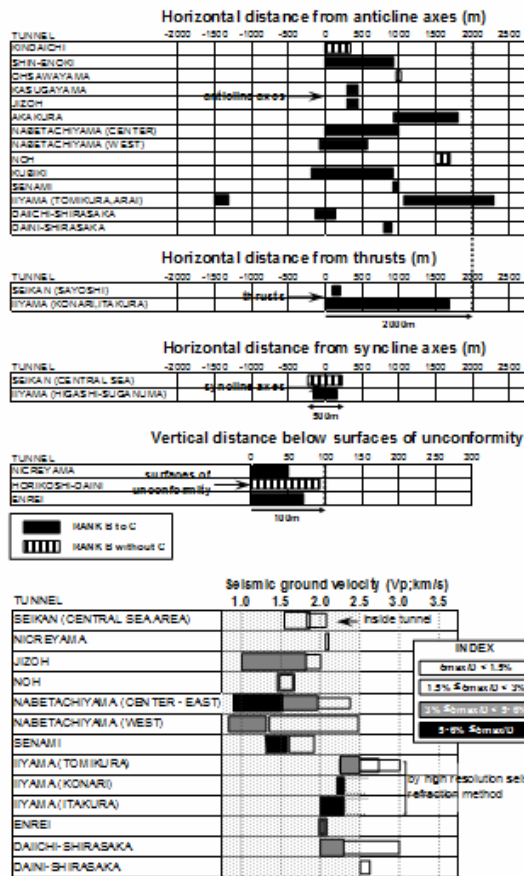$Gn < 2$ & $0.0435\gamma + 0.00928S + 0.0765Gn(=F) \leq 1$ ...(1)
$Gn < 2$ & $0.0435\gamma + 0.0765Gn (=F) \leq 1$ ...(2)

The competence factor (Gn) can be obtained from unconfined compressive strength / overburden pressure. In the case where the three parameters can be obtained, tunneling difficulty is judged to be likely when the Gn and F values are lower than the plain derived from equation 1) (see Figure 7A). In the case where sand content (S) cannot be obtained, tunneling difficulty is judged to be likely when the Gn and F values are lower than the lines derived from equation 2) (Figure 7B).

(shown in Figure 8). This geological structure is estimated through surface explorations, geophysical investigations and borehole surveys.

In order to determine the distribution of rock properties, the depth dependence of rock properties is estimated as shown in Figure 8C. Applying the criteria shown in equation 1), to the rock properties profile, the areas where the Gn and F values are lower than the criteria are judged to be difficult tunneling areas (Figure 8C). The areas with the wave pattern in this figure represent difficult tunneling areas, which are widely distributed in the Shiiya formation. According to the construction record shown in Figure 8D (Taketsu et al., 2003[3] and Nakamura et al., 2005[4]), areas judged to be difficult tunneling areas using the evaluation method correspond to areas where δmax (tunnel displacement)/D (tunnel diameter) is greater than 3%.
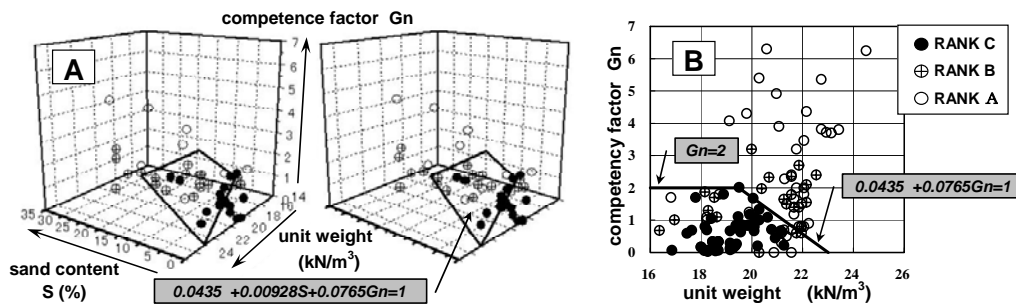

Figure 7 Criterion 3 for the case of mudstone - data from borehole logging

3.3 *Application of the evaluation method*

The evaluation criteria and method outlined above are applied to the case of the Iiyama tunnel, where data are available on the evaluation method and the results of construction and the application of the evaluation method can be verified. The target area is the northern part of the Iiyama tunnel, where the geological age of rock formations such as the Nishiyama, Shiiya and Haizume formations ranges from Tertiary to Quaternary. The Konari fault is located at the boundary between the Shiiya formation and the Haizume formation and disturbed zones are distributed around the derivative faults

4. PREDICTIVE EVALUATION OF ROCK BURST

4.1 *Procedure for the evaluation*

As shown in Figure 2, difficulties due to rock burst are limited to granitic formations in Japan. The evaluation procedure also consists of a surface exploration stage, a geophysical investigation stage and a borehole survey stage (Figure 9). Although the high probability area will be narrowed down in each investigation stage, the evaluation criteria in the first two stages are very simple and the criteria in the borehole survey stage are the main factors for predicting rock burst.
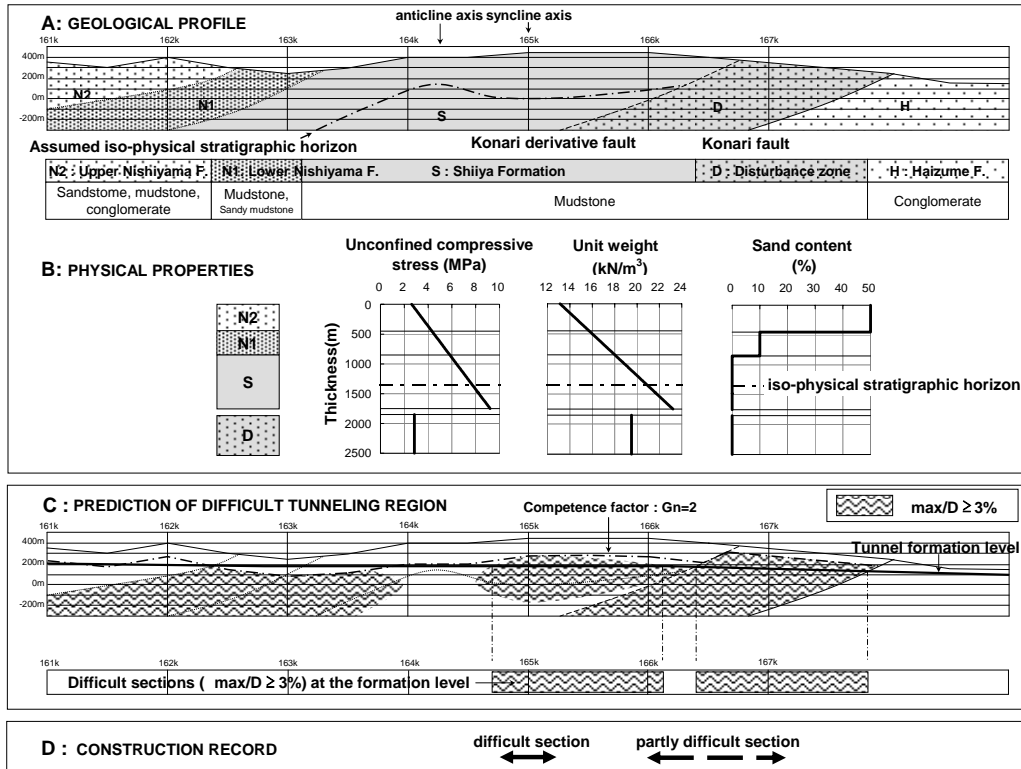
Figure 8 Evaluation results for prediction of squeezing ground in the case of mudstone

4.2 *Criteria for prediction of tunnelling difficulties in each stage*

Criteria for prediction of tunneling difficulties in each investigation stage are developed from indicators obtained from data on past tunneling difficulty due to rock burst. The criterion during surface exploration is whether the host rock is granitic or not (Figure 2) and, as shown in Figure 10, the criterion during the geophysical investigations is whether or not the elastic wave velocity is lower than 5 km/s (Ishiyama at al., 1991[5]).

In the borehole survey stage, the indicators for judging tunneling difficulty are in-situ stress, rock properties and the orientation of joint systems in the rock and the evaluation criteria are shown below.

(a) *Evaluation of in-situ stress*

According to tunnel construction records, in-situ stresses are measured using the stress release method in rock where rock burst has occurred. Although the stress release method is reliable for measuring in-situ stress, its application in deep borehole surveys is still in the development stage and the hydraulic fracturing method is mainly applied in deep borehole surveys. Therefore, the evaluation criteria for both the stress release method and the hydraulic fracturing method are discussed below.

- Stress release method

The relationships between rock burst and maximum (σ_1) / minimum (σ_3) principal stress measured using the stress release method are shown in Figure 11A. Whether rock burst occurs or not is clearly judged by the principal stress difference. However, rock burst is similar to borehole breakout
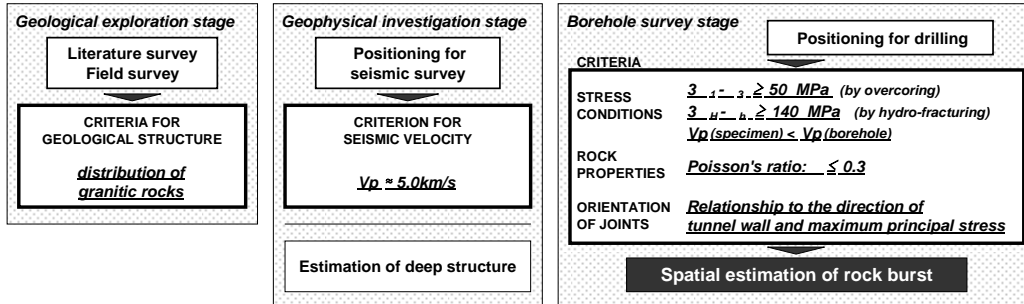
Figure 9 Evaluation stages and flow diagram for prediction of rock

TUNNEL or ROCK CLASSIFICATION	Rock name or type	Rock mass class or grade	Seismic ground velocity (Vp; km/s)
KANETSU T.	Quartz diorite		inside tunnel → ■■■■
KARISAKA T.	Granodiorite		Rock burst section
NISHIKAZE T.	Granite		
ROCK CLASSIFICATION FOR RAILWAY TUNNELS IN JAPAN*	Plutonic rock	VN IVN	
		IIIN	
		IIN	
ROCK CLASSIFICATION FOR HIGHWAY TUNNELS IN JAPAN*	Plutonic rock	A	
		B	
		CI	

*Japan Society of Engineering Geology (1992)[6]

Figure 10 Criterion 2 in the case of granitic rock - elastic wave velocity

and the evaluation criterion for borehole breakout conditions (Zoback et al., 1985[7]) is also used as an evaluation criterion for the differential stress condition.

Borehole breakout condition   : $3\sigma_1-\sigma_3 \geq 50\ MPa$
Differential stress condition   : $\sigma_1-\sigma_3 \geq 15\ MPa$
-    Hydraulic fracturing method

There are very limited relational data for rock burst and in-situ stress measured using the hydraulic fracturing method, because the hydraulic fracturing method is used mainly in deep borehole surveys where tunnels are not being constructed. However, according to borehole records for a depth of 2000 m (Tsukahara et al., 1996[8]), locations where rock burst occurred are close to locations where borehole breakout occurred. Therefore, the evaluation criteria for borehole breakout are applicable for rock burst. Relationships between borehole breakout and maximum (σ_H)/minimum (σ_h) horizontal stress are shown in Figure 11B. The evaluation criteria include difference in stress level as well as borehole breakouts, because rock burst will occur where the

difference between maximum and minimum stress is large.

Borehole breakout condition : $3\sigma_H-\sigma_h \geq 140\ MPa$
Differential stress condition   : $\sigma_H-\sigma_h \geq 30\ MPa$
-    Ultrasonic velocity for a test sample

According to previous R&D (Shimokawauchi at al., 1977[9]), the ultrasonic velocity (Vp) for a sample obtained from a geological formation where rock burst has occurred tends to be lower and is around 4 km/s, as shown in Figure 11C. It is assumed that large differential stress causes degradation of the sample through stress release and the decrease in ultrasonic velocity is related to the in-situ stress. Evaluation criteria for rock burst using ultrasonic wave velocity are shown below.

$Vp \geq 5.3km/s$ (decreased to around 4.0 km/s)

It is important to compare the ultrasonic wave velocities in-situ and for samples. Ultrasonic wave velocity depends on rock type and measuring the reduced velocity in the sample compared to velocity logging is therefore very important.

Borehole breakout condition $3\sigma_1-\sigma_3=50$MPa Differential stress $\sigma_1-\sigma_3=15$MPa
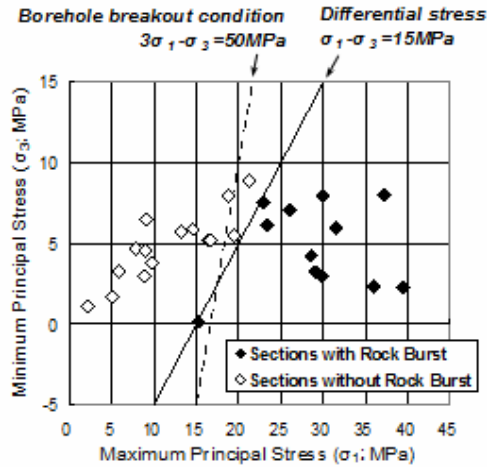
A: Overcoring Stress Measurements

Borehole breakout condition $3\sigma_H-\sigma_h=140$MPa Differential stress $\sigma_H-\sigma_h=30$MPa
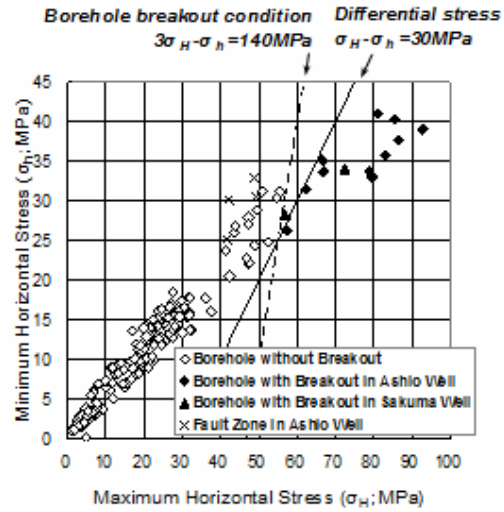
B: Hydraulic Fracturing Stress Measurements

C: Measurement of Ultrasonic Wave Velocity

Figure 11. Criterion 3 in the case of granitic rock – stress conditions
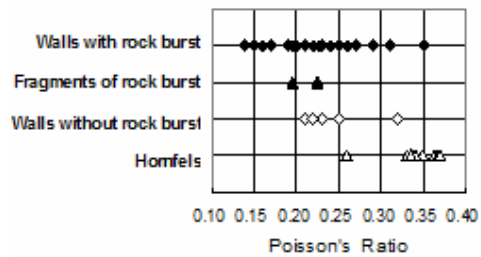
Figure 12. Criterion 3 in the case of granitic rock - physical properties

(b) Evaluation of rock properties

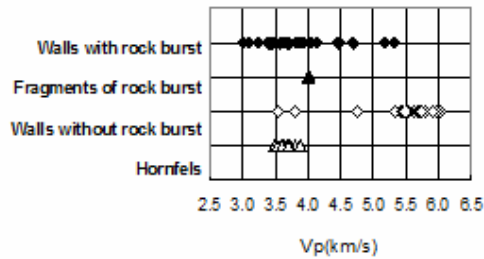According to construction records for the Kanetsu tunnel (Japan Highway Public Corporation, 1986[10]), rock burst occurs very rarely in granitic rocks bearing hornfels. Although there is no difference in unconfined compressive strength between granitic rocks and hornfels, the static Poisson's ratio of hornfels is higher than that of granitic rock (Figure 12). The static Poisson's ratio is used as an evaluation criterion for predicting rock burst as below.

Static Poisson's ratio   : $v \geq 0.3$

(c) Orientation of joints

The location of rock burst is often related to the direction of maximum in-situ stress and the orientation of joints, for example in the case of the Kanetsu tunnel, where rock burst occurred mainly in the tunnel face, as shown on the left side of Figure 13, and the Karisaka tunnel, where rock burst occurred at the roof, as shown on the right

side of Figure 13. Rock burst tends to occur if the directions of maximum principal stress and of the joint plane have a similar orientation. Therefore, the orientation of joints and the maximum principal stress is used as the evaluation criterion.

Sakuma area. In the SB-1 borehole, borehole breakout frequently occurred at depths greater than 800 m below ground surface.

According to the evaluation criteria for the hydraulic fracturing method, a depth of around 950 m is judged to be susceptible to rock burst. At a depth of more than 700 m below the surface, a
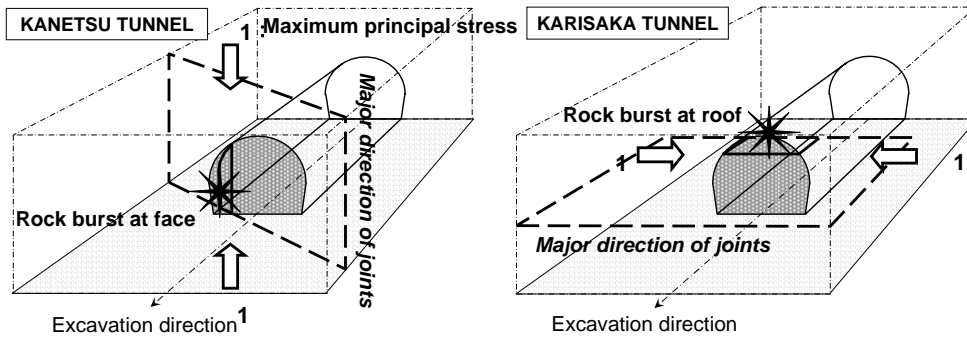
Figure 13 Criterion 3 in the case of granitic rocks – orientation of joint systems

4.3 *Application of evaluation method*

The evaluation method discussed above was applied to two 1,000 m depth borehole surveys (SB-1, 2) carried out in granitic rock in the Sakuma area located in the western part of Shizuoka Prefecture (New Energy Foundation, 2002[11]). Three types of granitic rock and hornfels are distributed in the

reduction in the ultrasonic wave velocity for core samples compared to in-situ measurements was observed. Based on these results, if a tunnel is constructed more than around 800 m below the surface (Figure 14), tunneling difficulty due to rock burst will occur. These results correspond with the area where borehole breakout occurred in a borehole survey.
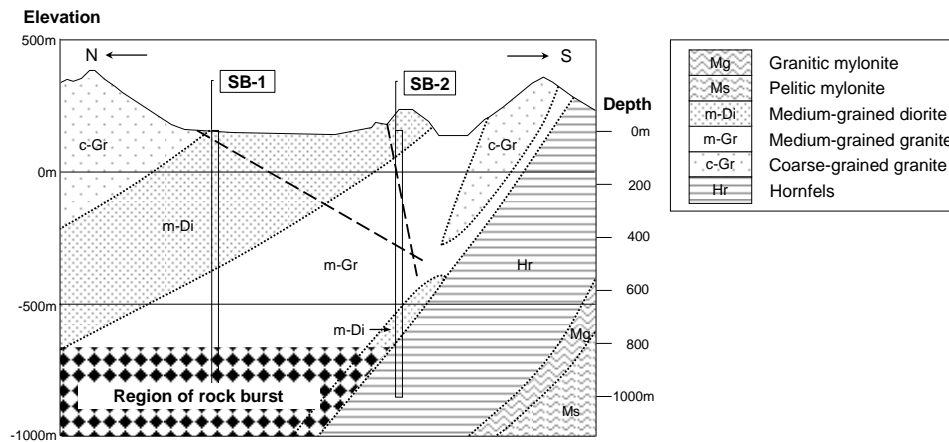
Figure 14 Evaluation results for prediction of rock burst in the case of granitic rock

5. CONCLUSIONS

In the preliminary investigation stage, the suitability of candidate sites for repository construction will be judged based on surface-based investigations such as geophysical surveys and a limited number of borehole surveys. Basic methods for predicting squeezing ground and rock burst are established. The suitability of the candidate site should be classified according to ease of construction, which may depend on the type of tunneling difficulty in question. It remains open how to classify tunneling difficulty. Although a method for prediction of squeezing ground in mudstone has been established, the evaluation methods for granite and tuff require further improvement. Additionally, it is necessary to establish a method for prediction of other difficulties arising during tunneling, such as large, high-pressure water inflow, collapse due to quicksand phenomena and generation of toxic gas.

ACKNOWLEDGEMENTS

REFERENCES

1. Shidahara, T., Kanazawa, S., Arai, T., Otsuka, M., Asakawa, M. and Tsuchi, H.: Study on capability of difficult work generation for selection of areas for detailed investigation. Proceedings of JSEG 2007FY annual study meeting, 32, pp.63-64, 2007. (In Japanese)

2. Kojima, Y., Asakura, T., and Yoshikawa, K.: Classification of squeezing muddy rock for NATM, Railway Technical Research Institute Report, vol.3, No.5, pp.47-53, 1989. (In Japanese)

3. Taketsu, E., Kojima, T. and Morita R.: Success over squeezing ground by multiple support construction method - Konari section of Iiyama tunnel on Hokuriku Shinkansen line, Tunnels and underground, Vol.34, No.8, pp.7-13, 2003. (In Japanese)

4. Nakamura, A., Tamai, T., Matsubara, T. and Morita, R.: Breakthrough of disturbance zone with abnormal squeezing phenomena by multiple support construction method - Iiyama tunnel on Hokuriku Shinkansen line (Konari and Itakura section), Tunnels and underground, Vol.36, No.7, pp.7-17, 2005. (In Japanese)

5. Ishiyama, K., Hirata, A. and Inaba, T.: Investigation with respect to rock burst occurred in excavation of tunnels, Nishimatsu technical research report, vol.14, pp.8-19, 1991. (In Japanese)

6. Japan Society of Engineering Geology: Rock mass classification in Japan, Engineering Geology, Special Issue, pp.3-12, 1992.

7. Zoback, M. D., Moos, D., Masten, L. and Anderson, R. N.: Well bore breakouts and in situ stress, J.Geophys.Res., 90, pp.5523-5530, 1985.

8. Tsukahara, H., Ikeda, R. and Omura, K. : In-situ Stress Measurements in an Earthquake Focus Area, Tectonophysics, No.262, pp.281-290, 1996

9. Shimokawauchi, M., Oda, S. and Kizawa, T.: An investigation from rock-burst phenomenon in Dai-Shimizu tunnel, Proceedings of 5th Japan Rock Mechanics Symposium, pp.70-84, 1977 (In Japanese)

10. Japan highway public corporation: Construction report of Kanetsu tunnel, 1986 (in Japanese)

11. New Energy Foundation: 2001FY research report on underground pumped power generation technology, 2002. (in Japanese)

BIOGRAPHICAL DETAILS OF THE AUTHORS

T. Shidahara graduated in Engineering Geology from the University of Tokyo in 1976. From 1976 to 2008 he worked for CRIEPI, Central Research Institute of Electric Power Industry, specializing in investigation for site selection and construction of hydraulic, nuclear and thermal power plants, as Senior Research Geologist from 1993. From 1991 he joined the research project for nuclear fuel cycle of CRIEPI, where he worked on geological aspects and rock quality evaluation for radioactive waste storage and disposal facility.

K. Shin graduated in Rock Mechanics from the University of Tokyo in 1983. He obtained a Ph.D. in Civil Engineering at the University of Tokyo. He has been working for the Central Research Institute of Electric Power Industry as a research engineer, specializing in tests, design and monitoring for underground rock cavern for pumped hydropower station. Present emphasis is on several projects related to underground disposal of nuclear waste in the field of site investigation, long term evaluation of the near field, and so on.
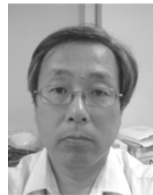
T.Arai graduated in Earth Science from the University of Ehime in 1983. From 1983 to 2004 he worked for Geotechnical Engineering Company, and established Geosphere Science Laboratory in 2004. He is specializing in geological and geotechnical consulting for construction of civil engineering structures. From 2002 he concerned with the research project for nuclear fuel cycle by CRIEPI, where he is engaged in geotechnical case study on the difficult tunneling works.

M. Asakawa graduated in civil Engineering from the University of Kyoto in 1995. From 1997 to 2005 he worked for the Kansai Electric Power Company. He experienced construction of coal thermal power station, design section, and planning section in the company. He moved to the Nuclear Waste Management Organization of Japan in 2005, working in International affairs and technical cooperation department.

M. Sawada graduated in Civil Engineering from the University of Tokyo in 2000. From 2000 to 2008 he worked for CRIEPI, Central Research Institute of Electric Power Industry, specializing in design and numerical simulation for underground facilities of hydraulic power plant and nuclear waste disposal.

Y. Inohara graduated in Earth Science from the University of Tokyo in 1978. From 1978 to now he worked for CRIEPI, Central Research Institute of Electric Power Industry, specializing in investigation for site selection and construction of hydraulic, nuclear and thermal power plants of Electric Utilities in Japan, as Senior Research Geologist. In 1990 he belonged to Nuclear Fuel Cycle Backend Research Center, CRIEPI, where he worked on geological aspects and rock quality evaluation for the radioactive waste storage and disposal facility.

D：熱－水－力耦合

D.1：Paper－In-situ heating test and thermal-hydro-mechanical coupled analysis in sedimentary soft rock for high level radioactive waste geological disposal

In-situ heating test and thermal-hydro-mechanical coupled analysis in sedimentary soft rock for high level radioactive waste geological disposal

Takafumi IKENOYA*, Tetsuji OKADA**, Masataka SAWADA**, Koichi SUZUKI**,
Kenji KUBOTA**, Nozomu TAKAKURA*, Yuichi TANAKA*, Kohei HIRANO***,
Kenji HIRAGA*** & Kazuo TANI****

Member of ISRM: Tokyu construction Co., Ltd., Shibuya-ku, Tokyo, 150-8340, Japan
*** Member of ISRM: Central Research Institute of Electric Power Industry, Abiko, Chiba, 270-1194, Japan*
**** Member of ISRM: Ceres Co., Ltd., Abiko, Chiba, 270-1194, Japan*
***** Member of ISRM: Yokohama National University, Hodogaya-ku, Yokohama, 240-8501, Japan*

ABSTRACT

Sedimentary soft rock is expected to be one of the potential host rock for the high level radioactive waste geological disposal. It is necessary to develop some evaluating methods for long-term stability of caverns in sedimentary soft rock which is sensitive for changes of environmental factors such as temperature and groundwater. Accordingly, in-situ heating test was conducted in an underground cavern at a depth of 50m for the purpose of improving thermo-hydro-mechanical coupled analysis code, and numerical results were compared with measured results.

The comparison between numerical and measured results for the heater's temperature of 90 °C is reported in this paper. Deformation of soft rock during the heating test was able to be broadly reproduced by numerical model considering linear elasticity and thermal expansion.

Keywords: High level radioactive waste, Geological disposal, In-situ test, Numerical analysis, Soft rock, Thermal expansion

1. INTRODUCTION

Sedimentary soft rock is expected to be one of the potential host rock for the high level radioactive waste geological disposal. It is predicted that rock mass around the disposal facilities will be heated by radionuclide decay in radioactive waste disposal. Long-term deformation characteristics of sedimentary soft rock can be affected by various environmental factors such as temperature and hydraulic conditions. Therefore, it is necessary to develop some evaluating methods for long-term stability of caverns in sedimentary soft rock in light of environmental factors change.

Accordingly, in-situ heating test was conducted in an underground cavern at a depth of 50m for the purpose of improving thermo-hydro-mechanical coupled analysis code, and numerical results were compared with measured results for the heater's temperature of 90 °C.

2. IN-SITU HEATING TEST

2.1 Site description

The underground test facility is located in a river terrace of 90m altitude, Sagamihara city, Kanagawa prefecture, and has a vertical shaft 50m deep. Figure 1 shows geological cross-sectional view of the site. In-situ heating test was conducted at a horizontal test adit called multidiscipline laboratory at a depth of 50m. Mudstone formation is distributed around the laboratory, and loosely cemented sandstone layers are also distributed thinly in the mudstone formation. Table 1 shows mechanical properties of the mudstone formation (Ochi et al., 1993).

2.2 In-situ heating test

Figure 2 shows cross-sectional view of the heating well. In the multipurpose laboratory, a heater well of 300mm diameter and 600mm deep was drilled and filled with groundwater. An electric heater was installed in the well for heating the surrounding rock mass via groundwater. Two agitators were installed in the well for keeping uniform distribution of temperature evenly during heating, and ground surface of the laboratory was covered with thermal insulant of expanded polystyrene for keeping boundary condition as adiabatic boundary.

Maximum heating temperature was set as 90 °C based on restrictive temperature of protector for high level radioactive waste geological disposal. Initial temperature in the heating well was 17 °C. First, groundwater in the heating well was heated to 40 °C. After equilibrium was reached of
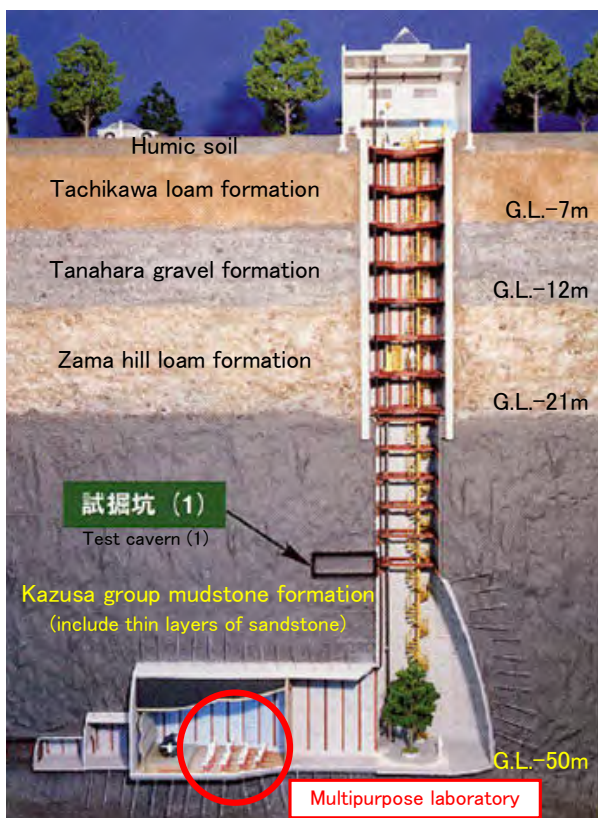
Figure 1. Geological cross-section and the location of the multipurpose laboratory

Table 1. Mechanical properties of mudstone formation.

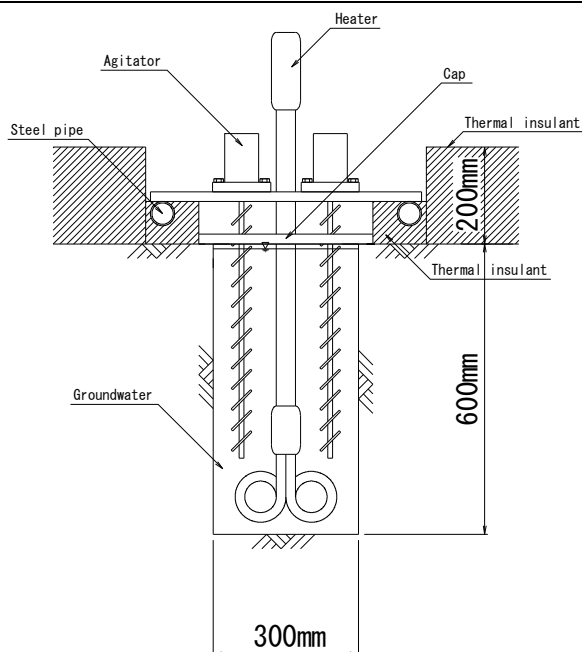| Mechanical properties	Symbol	Unit	Value
Moist unit weight	γ_t	kN/m^3	20.0
Uniaxial compression strength	q_u	MPa	5.6
Young's modulus	E_{50}	MPa	300
Young's modulus (at strains less than 0.0001%)	E_{max}	MPa	3,200
Coefficient of permeability	k	m/s	1.0×10^{-8}
Effective porosity	n_e	%	35

Figure 2. Cross-sectional veiw of the heater well.
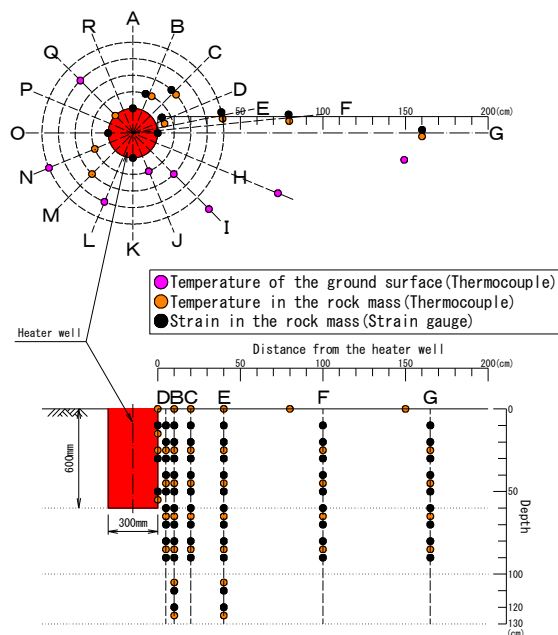
Figure 3. Arrangement of temperature and strain sensors. Upper: plan view, Lower: depth and distance from the heater well of sensors.

temperature and strain, groundwater was heated in stages, 60, 70, 90 °C.

Figure 3 shows the location of the temperature and strain sensors. During the heating, temperature and strain around the heater well were measured by the new instrument Core Sensor. Various sensors such as thermocouple and strain gauge and so on were fixed to a boring core taken from the depth of measurement. This core was backfilled with cement based backfilling material in the same place where the core was taken. The young's modulus of backfilling material was adjusted to that the surrounding mudstone formation.

2.3 Correction of measured strain

(a) Correction for gauge factor in data logger

Since the initial gauge factor in data logger is 2.00, strain is corrected by Equation (1).

$$\varepsilon_0 = \varepsilon \frac{2.00}{K} \tag{1}$$

where ε_0 : corrected strain, ε : measured strain, K : true gauge factor.

(b) Correction for sensitivity of wire lead

Since, the electric resistance of strain gauge changes by electric resistance and length of wire lead, the gauge factor is corrected by Equation (2).

$$K_0 = K \frac{R}{R + r \dfrac{L}{2}} \tag{2}$$

where K_0 : corrected gauge factor, R : electric resistance of

strain gauge (Ω), r : reciprocal electric resistance of wire lead per meter (Ω/m), L : length of wire lead (m).

(c) Correction of gauge factor for temperature change

Since gauge factor of strain gauge changes with temperature change, the gauge factor is corrected by Equation (3).

$$K_T = K\left(1 + C_k \frac{\Delta T_{cK}}{1000}\right) \tag{3}$$

where K_T : corrected gauge factor, C_k : temperature coefficient of gauge factor (%/10 °C), ΔT_{ck} : temperature difference from 20 °C (°C).

The following equation is divided from equation (2) and (3).

$$\varepsilon_i = \varepsilon_0 \frac{K_0}{K_T} \tag{4}$$

(d) Correction for thermal output

The strain output, when the object that strain gauge is fixed to is only strained by heat, is called thermal output, ε_{app}. This thermal output is described by Equation (5) in principle.

$$\varepsilon_{app} = \frac{\alpha}{K}\Delta T + \beta_s \Delta T - \beta_g \Delta T \tag{5}$$

where α : resistance temperature coefficient of strain gauge (ppm/°C), β_s : linear expansion coefficient of the object (μ/°C), β_g : linear expansion coefficient of strain gauge (μ/°C), ΔT : temperature difference (°C).

The first term in right side of Equation (5) is the apparent strain with electric resistance change of strain gauge by temperature change, the second term is thermal expansion of the object, and the third term is thermal expansion of strain gauge itself. Therefore, the terms except the second are must be removed from measurement data, since they are apparent strains

Usually, ε_{app} for the standard specimen is known as a function of temperature. And linear expansion coefficient of the standard specimen, β_s, is a known value such as 11.8μ/°C in case of SS400. Therefore, thermal output can be corrected as Equation (6) by subtracting the apparent strain described as Equation (5) from the measured strain. However, ε_{app} also must be corrected by Equation (1)~(4).

$$\varepsilon_c = \varepsilon_i - \left(\frac{\alpha}{K}\Delta T - \beta_g \Delta T\right) = \varepsilon_i - \left(\varepsilon_{app} - \beta_s \Delta T\right) \tag{6}$$

(e) Conclusions

The corrected strain, ε_c, is described as follows by substituting Equation (1)~(5) in Equation (6).

$$\varepsilon_c = \frac{2.00\varepsilon R}{K\left(R + r\frac{L}{2}\right)\left(1 + C_k \frac{\Delta T_{ck}}{1000}\right)} - \left(\frac{\alpha}{K}\Delta T - \beta_g \Delta T\right) \tag{7}$$
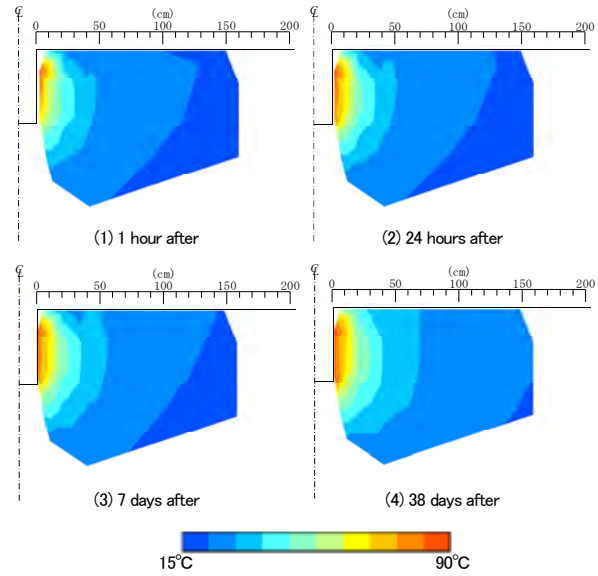

Figure 4. Distributions of temperature in rock mass.

2.4 Measurement result

Figure 4 shows temperature contour in the rock mass around the heater well when the heater temperature is 90 °C. The temperature shows the highest values, more than 70 °C in D hole, 5cm from the wall of heater well, and gradually with distance from the heater well. The increase of temperature of rock mass was 7~8 °C at 160cm from the heater well. These measured results are found similar to the predicted results by thermal-hydro-mechanical coupled analysis (Sawada et al., 2008). Moreover, it appears that the adiabatic boundary of ground surface was not kept completely and influenced by the air temperature in the laboratory, since temperature contour does not intersect orthogonally.

Figure 5 shows strains and temperatures histories in D hole, 5cm from the wall of heater well. Compressive strains are shown as positive. The measured strains were found extensive in every direction, and responding simultaneously with the changes of temperatures. Measured strains were as high as 600μ when the temperatures in the rock mass were the highest. Since the linear expansion coefficient of the mudstone formation is around 10μ/°C (Sawada et al., 2008) and the increase of temperature in the rock mass was around 54 °C, the expected strains by thermal expansion was calculated as 540μ. Therefore, a large part of the measured strains was attributed to the thermal expansion. Strains became smaller with distance from the heater well as is the case in temperature distribution.

3. THERMAL-HYDRO-MECHANICAL COUPLED ANALYSIS

3.1 Outline of numerical analysis

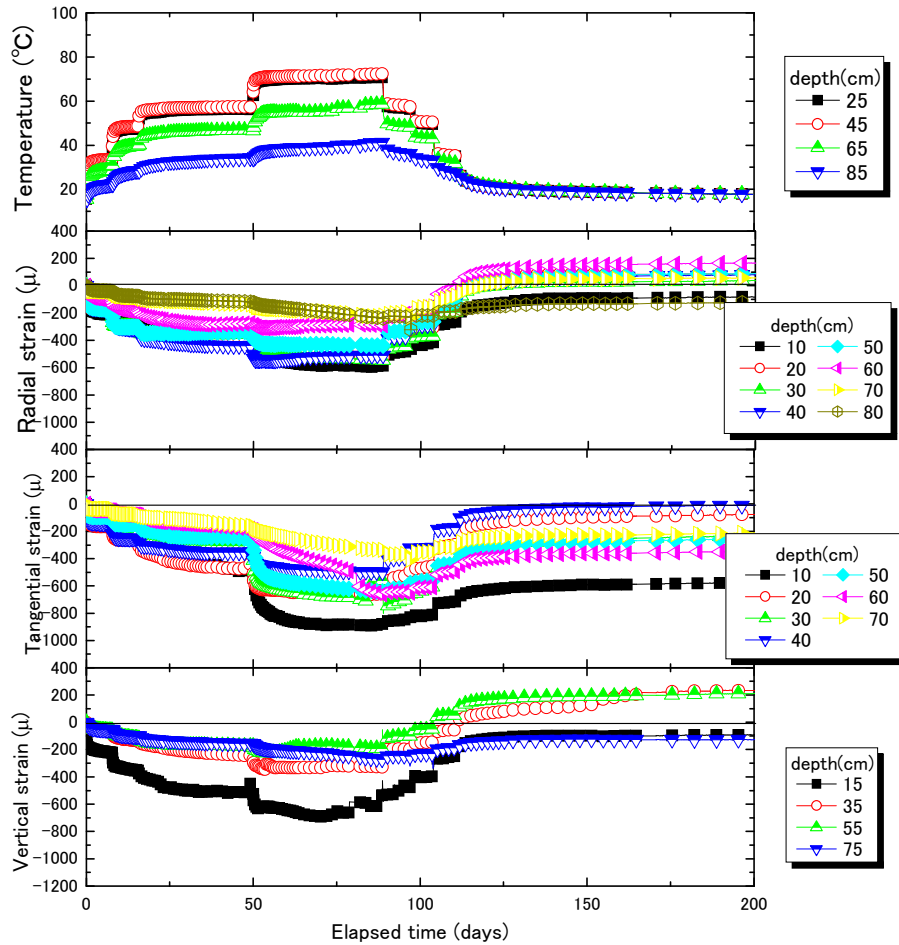Authors developed thermo-hydro-mechanical coupled

Figure 5. Strains and temperatures histories in D hole.

finite element analysis code, LOSTUF, for predicting long-term behavior of underground facilities influenced by heat and groundwater. In LOSTUF, ground is modeled as multi-phase system where voids of the skeleton are filled partially with liquid water and partially with gas. Governing equations are derived from mass conversation of water, energy conversation, momentum balance, and various constitutive laws. Pore gas pressure is assumed to be constant and equal to the atmospheric pressure. Here, governing equations used in LOSTUF are briefly described.

The water mass flow equation is derived as follows,

$$\rho_l S_l \frac{\partial(\nabla \cdot \boldsymbol{u})}{\partial t} + \rho_{l0}\phi S_l \beta_{Pl}(\rho_l - \rho_v)C_{lP}\frac{\partial P}{\partial t}$$

$$-(\rho_{l0}\phi S_l \beta_{Pl} - \rho_l C_{vT})\frac{\partial T}{\partial t} + \nabla \cdot \left[\left(-\rho_l \frac{\boldsymbol{k}k_{rl}}{\mu_l} - \rho_l D_{Pv}\boldsymbol{I}\right)\nabla P\right]$$

$$+\nabla \cdot [(-\rho_l D_{Tv}\boldsymbol{I})\nabla T] = Q_B + \nabla \cdot \left(\rho_l \frac{\boldsymbol{k}k_{rl}}{\mu_l}\boldsymbol{g}\right) \qquad (8)$$

where ρ_l : liquid water density, ρ_v : vapor water density, S_l : liquid water saturation, $\rho_{l\,0}$: initial density of water, ϕ : porosity, β_{Pl} : compressibility of water, β_{Tl} : linear thermal expansion coefficient of water, k : intrinsic permeability

tensor, k_{rl} : relative permeability for water, $\boldsymbol{I}$: indentity tensor, $\boldsymbol{g}$: gravity acceleration vector, Q_B : source term of groundwater, $\boldsymbol{u}$: displacement vector, P : pore water pressure, T : temperature, C_{lP} : isothermal liquid water capacity, C_{vT} : thermal vapor water capacity, D_{Pv} : isothermal vapor diffusion coefficient, and D_{Tv} : thermal vapor diffusion coefficient. D_{Pv} and D_{Tv} are functions of temperature and water saturation. But in the analysis of this heating test, terms including these coefficients are ignorable because ground was saturated.

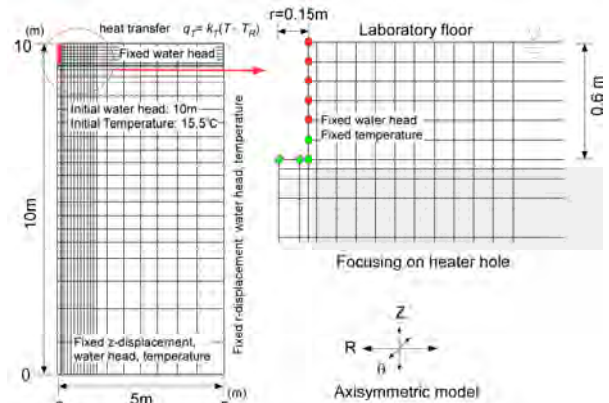The energy equation is obtained as follows,

Figure 6. Finite element mesh and boundary conditions.

Table 2. Material properties for numerical analysis.

Mechanical properties	Symbol	Unit	Value
Average density of mixtrue	ρ_m	g/cm^3	2.0
Young's modulus	E_{50}	MPa	1400
Poisson's ratio	ν	-	0.3
Initial void ratio	e_0	-	0.6
Eigen transmittance	k	m^2	1.0×10^{-15}
Specific heat of solid phase	c_s	J/kgK	740
Specific heat of water	c_l	J/kgK	4200
Thermal conductivity of solid phase	λ_s	W/mK	1.60
Thermal conductivity of water	λ_l	W/mK	0.58
Linear thermal expansion of solid phase	β_{TD}	1/K	1.0×10^{-5}
Linear thermal expansion of water	β_{Tl}	1/K	5.0×10^{-4}
Compressibility of water	β_{Pl}	1/MPa	5.0×10^{-4}

$$[(1-\phi)3K_D\beta_{TD}T]\frac{\partial[\nabla\boldsymbol{u}+(\nabla u)^{tr}]}{\partial t}+(\rho c)_m\frac{\partial T}{\partial t}$$

$$+\nabla\cdot\left\{\phi S_l\left[T\left(\frac{\beta_{Tl}}{\beta Pl}\right)\frac{\boldsymbol{k}k_{rl}}{\mu_l}+\rho_l LD_{Pv}I\right]\nabla P\right\}$$

$$-\nabla\cdot(\lambda_m\boldsymbol{I}\nabla T)+(c_l q_l)\cdot\nabla T=Q_{TB} \tag{9}$$

where K_D : drained bulk modulus of medium, β_{TD} : drained linear thermal expansion coefficient of the medium, L : latent heat of vaporization of water, λ_m : apparent macroscopic thermal conductivity of mixture, $(\rho C)_m$: thermal content of mixture. λ_m and $(\rho C)_m$ are obtained from following equations.

$$\lambda_m=\phi S_l\lambda_l+(1-\phi)\lambda_s \tag{10}$$

$$(\rho c)_m=\phi S_l\rho_l c_l+(1-\phi)\rho_s c_s \tag{11}$$

where, λ_l : thermal conductivity of water, λ_s : thermal conductivity of solid phase, c_l : specific heat of water,
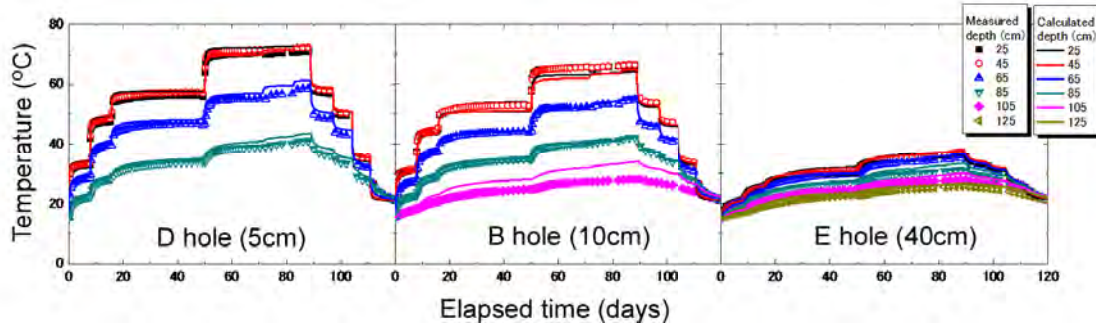

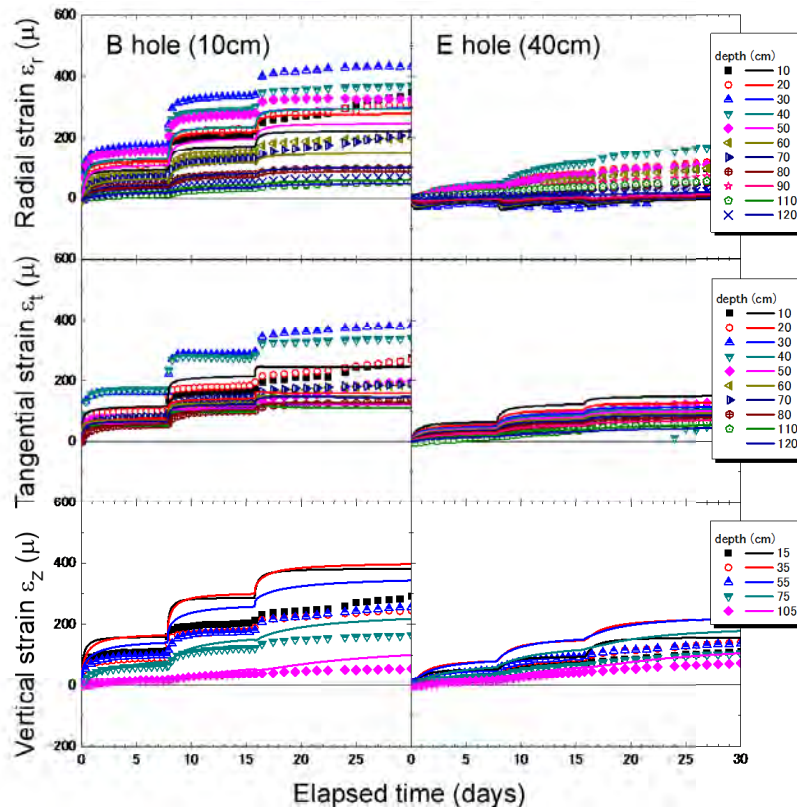Figure 7. Temperature histories in D hole, B hole, and E hole.

Figure 8. Radial, tangential, and vertical strain histories in B hole and E hole.

ρ_s:density of solid phase.

Stress equilibrium is obtained as follows,

$$\nabla \cdot \left\{ \boldsymbol{D} : \frac{\partial \left[\nabla \boldsymbol{u} + (\nabla \boldsymbol{u})^{tr} \right]}{\partial t} \right\} + \nabla \cdot \left(-\boldsymbol{I} \chi \frac{\partial P}{\partial t} \right)$$

$$+ \nabla \cdot \left[(-\boldsymbol{D} : \boldsymbol{I} \beta_{TD}) \frac{\partial T}{\partial t} \right]$$

$$= \frac{\partial}{\partial t} (\rho_m \boldsymbol{g}) + F_B \qquad (12)$$

where $\boldsymbol{D}$: stiffness tensor. If ground is assumed as isotropic linear elastic body, $\boldsymbol{D}$ is defined by Young's modulus E and Poisson's ratio v. χ : Bishop's effective stress factor, ρ_m : average density of the mixture, and F_B : external force term. In LOSTUF, we can use various mechanical constitutive models such as linear elastic, nonlinear elastic, cleep of soft rock, elasto-viscoplastic model of clay, Cam-clay model and so on.

3.2 Numerical model and material properties

Figure 6 shows finite element mesh and boundary conditions. Numerical analyses were conducted by axisymmetric model. Analytical region is 5m of radial length and 10m of height and are divided to 560 finite elements and 609 nodes. Heat transfer boundary was given on top surface, and heat transfer coefficient was 23.26 W/m²K, since adiabatic condition was not achieved on laboratory floor. Table 2 shows the material properties for numerical analysis.

4. COMPARISON BETWEEN NUMERICAL RESULT AND MEASRUED RESULTS

Figure 7 compare the calculated and measured temperatures histories in D hole, B hole and E hole. It appears that the differences between numerical results and measurements were less than 3 °C.

Figure 8 compares the calculated and measured strains in B hole and E hole. Directions of strains are radial, tangential and vertical. Both calculated and measured strains in every direction showed a trend of tension, that is volume expansion probably due to heating. Although some differences of strains were observed between numerical results and measured, the numerical results generally agreed well with the measured results. Calculated vertical strains were greater than measured strains in both holes. Although it is easy to deform vertically because the boundary condition of ground surface is free in numerical analysis, measured vertical strains were not larger than calculated stains actually. The heating test could be influenced by initial earth pressure, the shape of the laboratory, excavation history and so on. Thus these factors must be included in numerical model.

5. CONCLUSIONS

In-situ heating test and thermo-hydro-mechanical coupled analysis were carried out to develop evaluating method for long-term stability of caverns in sedimentary soft rock. Although adiabatic boundary at the ground surface in the multipurpose laboratory was not kept completely, the numerical analysis could successfully reproduce the temperature changes with time by assumption of heat transfer boundary and isotropic linear elastic body. Since the measured results were influenced by initial earth pressure, the shape of the laboratory, excavation history, and so on, further development is needed to include these factors for the numerical analysis.

REFERENCES

Ochi, K., Tsubouchi, T. and Tatsuoka, F., 1993. Deformation characteristics of sedimentary soft rock examined by the excavation of deep shaft and field tests, *Journal of Geotechnical Engineering*, No.463/III-22, pp.143-152 (in Japanese).

Sawada, M., Takeda, K., Tani, K., Okada, T., Takakura, N., Ikenoya, T., 2008. Thermo-hydro-mechanical coupled analysis for preliminary investigation of in-situ heater test in sedimentary soft rock, *Proc. of the 37th Sym. on Rock Mechanics*, pp.283-288 (in Japanese).

Katto, Y., 1964. General remarks of heat transfer, Yokendo Co., Ltd (in Japanese).

D.2：Paper－Thermo-hydro-mechanical model of the

Canister Retrieval Test

Thermo-hydro-mechanical model of the Canister Retrieval Test ☆

M.T. Zandarin [a], A. Gens [b,*], S. Olivella [b], E.E. Alonso [b]

[a] Universitat Politècnica de Catalunya, Barcelona, Spain
[b] Civil Engineering, Universitat Politècnica de Catalunya, Barcelona, Spain

ARTICLE INFO

ABSTRACT

The paper presents a 2-D axisymmetric numerical simulation of the Canister Retrieval Test (CRT). The main objectives of this analysis are the study of the canister–buffer and buffer–host rock interfaces; and the evaluation of the mathematical models used to predict the THM behaviour of the buffer and interface. The THM simulation was performed using the finite element program Code-Bright. The constitutive law adopted to represent the mechanical behaviour of bentonite and pellets is the Barcelona Basic Model (BBM) with a non-linear elastic component accounting for swelling. A joint element with a non-linear elastic mechanical law was implemented in the code for the simulation of the opening–closure of the interface canister–buffer. The formulation of this element also incorporates appropriate thermal and hydraulic laws. The evolution of temperatures, relative humidities and stresses recorded during the test were compared with the simulation results. Comparing the results measured in situ with the results of numerical analysis shows that the formulation used is able to reproduce satisfactorily the phenomena involved in the test as well as their interactions. In addition, the final dry density and degree of saturation measured in samples of bentonite and pellets extracted during the test dismantling were also in agreement with the calculated values.

© 2011 Elsevier Ltd. All rights reserved.

1. Introduction

The main objective of the Canister Retrieval Test (CRT) was to demonstrate that retrieval of canisters is technically feasible at any stage of the operating phase. In addition, the CRT experiment has also been used to carefully record the THM processes in the Swedish KBS-3V deposit arrangement. This makes it very suitable for modellers to investigate the formulations used in the simulations, as the calculated results can be checked against experimental data.

The CRT experiment has been numerical modelled in the context of the THERESA (Thermo-Hydrological–Mechanical–Chemical processes for application in repository safety assessment) European research project. In this paper the THM behaviour of interfaces present between canister and engineered buffer and the homogenisation of the engineer barrier formed by bentonite blocks and a pellet-filled slot are considered.

The paper starts with a description of the geometry and protocol of the Canister Retrieval Test. The THM formulation adopted to perform the simulation and the determination of materials parameters is then presented. Afterwards, the numerical results obtained from the simulation of the test are compared with the experimental data. Finally, a discussion of the results is presented followed by some conclusions.

2. Description of Canister Retrieval Test

The Canister Retrieval Test is a full scale in situ test heating that involved the placement of a full-scale canister in vertical drifts surrounded by an engineered barrier. A view of the experimental geometry is given in Fig. 1b extracted from Börgesson (2007).

The deposition tunnel for the experiment is located in the 420-m level of the Aspö underground laboratory and was excavated by conventional drill and blast. It has an approximately 6 × 6 m horseshoe-shaped section. Two deposition boreholes were bored with a full-face tunnel boring machine modified for drilling vertical boreholes. The deposition borehole is 8.55 m deep and has a diameter of 1.76 m. The surrounding rock at the upper part of the borehole consists mainly of greenstone and the lower part of Äspö diorite. One of the boreholes has been used for Canister Retrieval Test (CRT). The other borehole was used to perform the Temperature Buffer Test (TBT). The experiments, CRT and TBT, are placed approximately at the tunnel centreline. The centre-to-centre distance between the two deposition boreholes is 6 m, which is the spacing being considered for the deep repository (Fig. 1a).
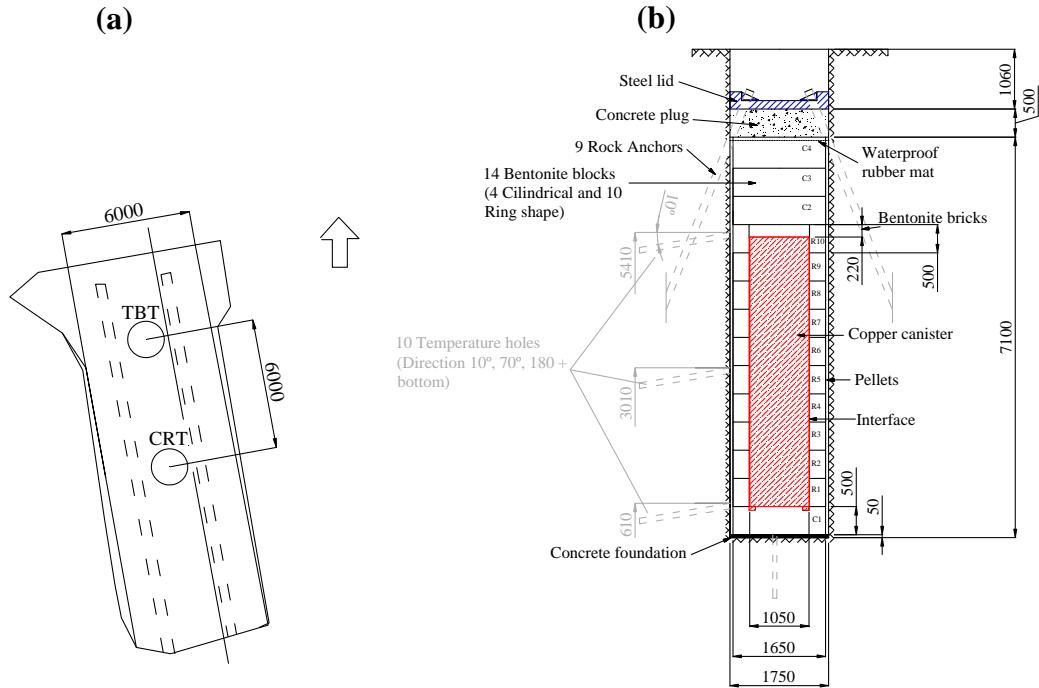
Fig. 1. (a) Location of TBT and CRT in the TASD tunnel of the Aspö underground laboratory. (b) Canister Retrieval Test geometry (Börgesson, 2007).

In the CRT borehole a 0.15 m high concrete foundation was built to prevent the water leaking from the rock from reaching the bentonite blocks and thereby to reduce the risk of tilting the stack of bentonite rings. Slots were cut in the rock wall for cables to prevent them being damaged. Also 16 filter mats with a width of 10 cm are installed adjacent to the rock wall with uniform spacing, starting 0.15 m from the borehole bottom up to a 6.25 m height.

The bentonite used as buffer material is SKB's reference buffer material, named MX-80. The buffer consists of highly compacted bentonite blocks and rings with an initial dry density of 1710 and 1790 kg/m^3, respectively. The initial water content of the bentonite was 17.3–16.7% with a mean value of 17%. The bentonite buffer was installed in form of blocks and rings of bentonite. The blocks have a diameter of 1.65 m and a height of 0.5 m. Ring-shaped or cylindrical bentonite blocks are placed in the borehole. When the stack of blocks was 6 m high, the canister, equipped with electrical heaters, was lowered down in the centre of the borehole and the cables to the heaters and instruments were connected.

A canister obtained from SKB's Encapsulation Project was used in the Canister Retrieval Test. The outside diameter of the canister is 1050 mm. The height of the canister is 4.83 m and the weight 21.4 tonnes.

At the top of the canister, MX-80 bentonite bricks fill up the volume between the canister top surface and the top surface of the upper ring (R10). The height difference between the two surfaces was 220–230 mm. The space between the bentonite blocks and the borehole wall is filled with bentonite pellets and water. Additional blocks were emplaced until the borehole was filled to a distance of one metre from the tunnel floor.

The top of the borehole was sealed with a retaining structure formed by a plug made of concrete, a steel lid and rock anchors. The aim of the structure is to prevent the blocks of bentonite from swelling uncontrollably.

An impermeable rubber mat was installed between bentonite block C4 and the concrete plug. On top of the plug the steel lid was installed. The plug and lid can move vertically and are attached to the rock by nine rock anchors. Each of the nine rock anchors consists of 19 steel wires with a nominal area of 98.7 mm^2

having 5 m fixed length and 5 m free length. The inclination of the anchors is 2.5:1, approximately 22° (Fig. 1b) (Thorsager et al., 2002; Börgesson, 2007).

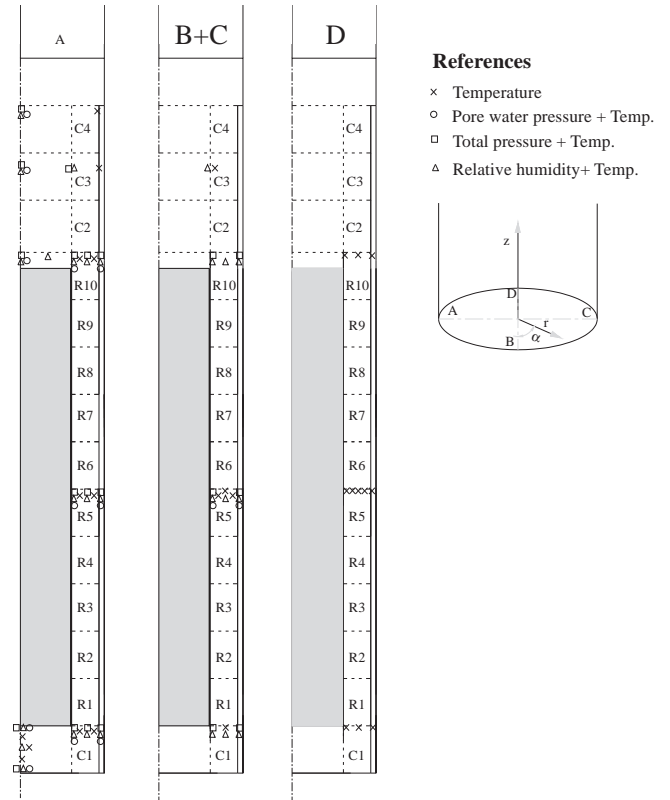A large number of instruments were installed to measure the following variables:

Fig. 2. Schematic view of the sensor locations in the Canister Retrieval Test (Börgesson, 2007).
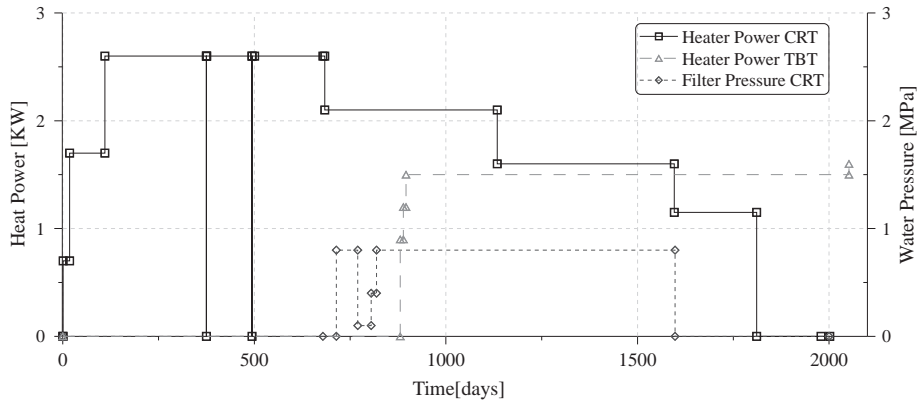
Fig. 3. Graph of the heat power protocols of CRT and TBT and the filter pressure protocol of CRT (Börgesson, 2007).

- Canister – temperature and strain.
- Rock mass – temperature and stress.
- Retaining system – force and displacement.
- Buffer – temperature, relative humidity, pore pressure and total pressure.

The instrumented sections are indicated in Fig. 2. The positions of the instrument in the buffer are indicated as follows: bentonite ring or cylinder number counted from the bottom/direction A (180°), B (0°), C (270°) or D (90°)/radial distance from centre line in mm. The identification of the sensors in the rock is as follows: distance in metres from the bottom/direction according to Fig. 2/ distance in metres from the borehole surface.

Temperatures were measured using thermocouples. Relative humidity was determined using Wescor psychrometers and capacitive transducers manufactured by Vaisala. Total pressures were recorded using Geokon transducers (Börgesson, 2007).

3. Test protocol

1. The starting date of the experiment was October 26, 2000 (00-10-26) when the buffer–rock interface was filled with pellets. Afterwards, water was pumped into the gap and filter mats.
2. Once pellets were hydrated the concrete plug was cast and heating started. Heating began with an initially applied constant power of 700 W at day 1.
3. When the concrete plug rose 13 mm due to bentonite swelling three rock anchors were locked on day 5. The initial force in each anchor was 20 kN.
4. The canister heating power was raised twice, at day 18 to 1700 W and at day 110 to 2600 W.
5. When the total force exceeded 1500 kN, the remaining six anchors were fixed. This procedure took place on days 46–48. The total force where distributed equally between all anchors, about 170 kN/anchor.
6. The water pressure at filter mats was increased gradually up to 0.8 MPa from day 679 to 714 (02-09-05 to 02-10-10). On day 770 the water pressure was decreased to 0.1 MPa. Then it was increased again up to 0.8 MPa on day 819 (03-01-23) and remained constant until day 1598 (05-03-12), then the water pressure was removed.
7. Heating of TBT was started at day 881 (03-03-26). This heating affected sightly the temperature of the CRT buffer.
8. The heating was switched of on day 1811 (05-10-11). After the end of test, several samples from the buffer were drilled to measure their dry density and degree of saturation. (Börgesson, 2007)

Fig. 3 shows a summary of the heat power and filter pressure protocol followed in the CRT and TBT tests.

4. Features of the analysis and material parameters

The analysis has assumed axisymmetric conditions using the mesh shown in Fig. 4. The materials considered in the model are bentonite, discriminating between cylinders, rings and bricks; pellets, the interface between bentonite and canister, canister, the concrete plug, the steel lid and the air in the gallery.

The geometry is discretized by 4-noded quadrilateral structured elements, and the mesh includes 1449 elements and 1540 nodes; 80 elements correspond to interface elements (indicated in Fig. 4).

The initial porosity (n_0), temperature and degree of saturation (Sr) of bentonite, pellets and interface have been obtained from Johannesson (2007) (see Table 1). The initial temperature for the air gallery is equal 15 °C and for the other materials are 20 °C
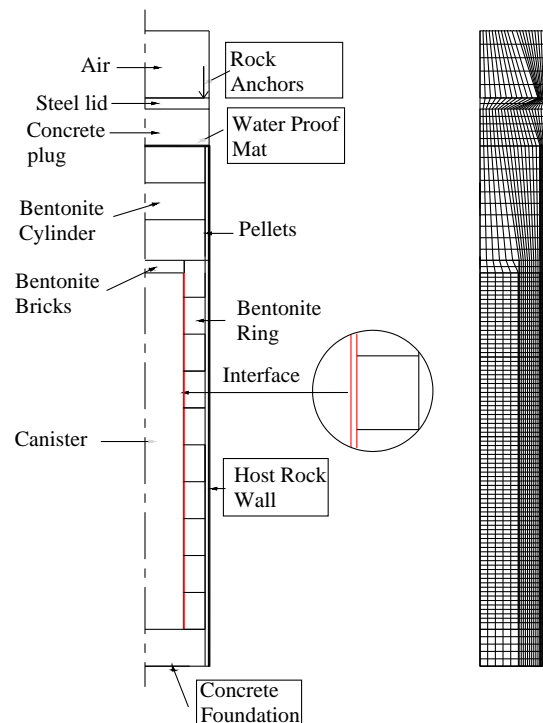

Fig. 4. Geometry and materials of CRT considered for the numerical model and finite element mesh used for discretization.

Table 1
Initial conditions and thermo-hydro-mechanical properties of materials considering in the model.

Material	Initial conditions				Thermal properties			Hydraulic properties					Mechanical properties	
	n_0	ρ_d (kg/m³)	Sr (%)	Pl_0 (MPa)	λ_{dry} (W/mK)	λ_{sat} (W/mK)	α (°C⁻¹)	k_0 (m²)	P_0 (MPa)	λ	P_d (MPa)	λ_d	Elastic parameter	Visco-plastic parameter
Bentonite cylinder	0.39	1699	75.1	−43.1	0.3	1.3	3.2×10^{-6}	3.50×10^{-21}	30	0.2	500	1.1	$\kappa_{i0} = 0.032$; $\kappa_{s0} = 0.072$; $\alpha_i = -0.008$; $\alpha_{sp} = -0.0016$; p_{ref} (MPa) = 0.1; G (MPa) = 2.48	Γ_0 [s⁻¹] = 1×10^{-4}; $N = 5$; $F_0 = 1.0$; $\lambda_{(0)} = 0.15$; $r = 0.4$; $\beta = 0.03$; $M = 1.0$; $\alpha = 0.3$; $p^*_0 = 4.0$; $p_c = 0.1$
Bentonite ring	0.36	1782	85.9	−28.6				2.60×10^{-21}	50	0.3	600	1.1		
Bentonite bricks	0.42	1616	63.7	−42.6				4.67×10^{-21}	20	0.22	300	1.1		
Pellets	0.64	1001	89.5	−3.4	0.1	1.1	3.2×10^{-6}	3.90×10^{-19}	5	0.2	600	1.1	$\kappa_{i0} = 0.074$; $\kappa_{s0} = 0.003$; $\alpha_i = -0.003$; $\alpha_{sp} = -0.006$; p_{ref} (MPa) = 0.1; G (MPa) = 1.05	Γ_0 [s⁻¹] = 1×10^{-4}; $N = 5$; $F_0 = 1.0$; $\lambda_{(0)} = 0.15$; $r = 0.425$; $\beta = 0.03$; $M = 1.0$; $\alpha = 0.3$; $p^*_0 = 0.3$; $p_c = 0.095$
Interface	–	1000	100.0	−0.1	0.1	1.3	–	1.00×10^{-16}	1	0.3	–	–	m (MPa) = 1.0; K_t (MPa/m) = 1.0×10^6; a_0 (m) = 0.01	
Canister	0.001	8000	–	−0.1	100	100	12×10^{-6}	1.00×10^{-30}	1000	0.5	–	–	E (MPa) = 130×10^3; $\upsilon = 0.25$	
Concrete plug	0.001	2400	–	–	2.7	2.7	10×10^{-6}	1.00×10^{-30}	1×10^{-6}	0.5	–	–	E (MPa) = 30×10^3; $\upsilon = 0.15$	
Steel lid	0.001	7840	–	–	47	47	12×10^{-6}	1.00×10^{-30}	1×10^{-6}	0.5	–	–	E (MPa) = 206×10^3; $\upsilon = 0.3$	
Air	0.98	1000	–	–	0.03	0.03	–	1.00×10^{-30}	1×10^{-6}	0.5	–	–	E (MPa) = 0.02; $\upsilon = 0.25$	

(The difference between temperatures is due to the gallery ventilation). The initial liquid pressures (Pl_0) were calculated considering the retention curves of the materials and their saturation degrees as measured in the tests. The retention curve obtained from the laboratory tests were fitted with the model proposed by Sánchez (2004), see Fig. 7. Initial total stress of the materials is assumed isotropic and equal to 0.11 MPa. A constant gas pressure equal to atmospheric was assumed throughout the test. The initial conditions of the materials are summarised in Table 1.

The heater power was applied over the canister volume according to the test protocol without considering the falls of heat power to zero on days 375 and 494 (Fig. 3). A special boundary condition was prescribed in the host rock to allow some energy flux. The energy flux is expressed as an outflow rate given by:

$$j_e = j_e^0 + \gamma_e(T^0 - T) + E_g^w(j_g^w) + E_l^w(j_l^w) \tag{1}$$

where γ_e is a leakage coefficient. This parameter was calibrated to obtain the temperature measured by sensors at the host rock wall. Also, this boundary condition allows considering the influence of the heating from the TBT experiment.

The filter pressures shown in Fig. 3 were applied at the host rock wall. The bottom boundary of the Cylinder 1 and the top of Cylinder 4 were considered impervious because of the presence of concrete foundation and a rubber mat respectively.

The force applied on the steel lid by the anchors was considered as point load acting on the steel lid (Fig. 4). The point load was calculated from the total force measured in the steel lid (1500 kN).

5. Materials parameters

5.1. Thermal properties

The thermal conductivity is given by:

$$\lambda = \lambda_{sat} \sqrt{S_l} + \lambda_{dry}\left(1 - \sqrt{S_l}\right) \tag{2}$$

where λ_{sat} is the thermal conductivity for a degree of saturation $S_l = 1$ and λ_{dry} is the thermal conductivity for a $S_l = 0$.

The parameters λ_{sat} and λ_{dry} for bentonite and pellets were determined fitting the experimental data with Eq. (2) (Fig. 5a and b). The thermal conductivities of canister, concrete plug and steel lid were given in Börgesson et al. (1994, 1995) and Sugita et al. (2003). For the interface, the conductivities adopted were similar to those of bentonite, because during the test the bentonite expands filling the interface space. Also the specific energy of the solid phase and the thermal expansion coefficients of bentonite, pellets are given in Börgesson et al. (1995). The properties for canister, concrete plug and steel lid were given in Börgesson (2007). The thermal parameters are listed in Table 1.

5.2. Hydraulic properties

The hydraulic conductivity of the materials is given by:

$$\mathbf{K}_l = \frac{\mathbf{k}k_{rl}\rho_l g}{\mu_l} \tag{3}$$

where k is the intrinsic permeability; k_{rl} is the relative permeability; ρ_l is the liquid density; μ_l is the viscosity of the liquid and g is the gravitational force.

The intrinsic permeability depends on porosity according to:

$$\mathbf{k} = k_0 \frac{n^3}{(1-n)^2} \frac{(1-n_0)^2}{n_0^3}\mathbf{I} \tag{4}$$

where k_0 is the reference intrinsic permeability at the reference porosity n_0.
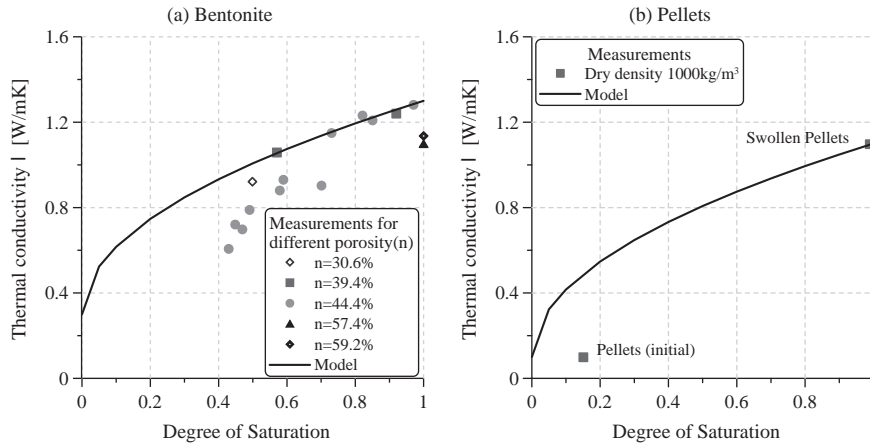
Fig. 5. Variation of bentonite and pellets thermal conductivity with degree of saturation. Experimental results and model fitted (Börgesson and Johannesson, 1995; Sugita et al., 2003).

The intrinsic permeabilities at different porosity of MX-80 bentonite and pellets were experimental measured by Pusch (2001), Villar (2002, 2003), Börgesson and Hernelind (1999), Imbert et al. (2004) and Lajudie et al. (1994). Fig. 6 shows the values of intrinsic permeabilities adopted for bentonite cylinders, rings, bricks and pellets. For the interface element, a constant permeability five orders of magnitude higher than bentonite was adopted. This greater permeability was considered adequate to model the high conductivity of the interface that has a thickness of 1 cm.

For the canister, steel lid and air very low permeabilities compared to bentonite permeabilities were used (Table 1).

The relative humidity of the liquid phase is given by:

$$k_{rl} = S_{el}^n \tag{5}$$

where S_{el} is the effective degree of saturation and n is a parameter of the model. In this case a value $n = 3$ has been adopted. This power function has been found to be adequate for modelling bentonite. This function and value of n were determined from back-calculation of hydration tests on bentonite (Pintado et al., 2002). The effective degree of saturation is evaluated as:

$$S_{el} = \frac{S_l - S_{lr}}{S_{ls} - S_{lr}} \tag{6}$$

where S_{lr} is the residual saturation; S_{ls} is the maximum saturation and S_l is the liquid degree of saturation which is calculated by the retention curve.

The retention curve adopted in the analysis for MX-80 bentonite and pellets is a modification of the Van Genutchen expression (1978) proposed by Sánchez (2004).

$$S_l = \left[1 + \left(\frac{\psi}{P}\right)^{\frac{1}{1-\lambda}}\right]^{-\lambda} f_d \quad f_d = \left(1 - \frac{\psi}{P_d}\right)^{\lambda_d} \tag{7}$$

where ψ is the total suction; P is the capillary pressure; λ is a model parameter and f_d is a function included to properly fit the high-suction range of experimental data obtained. P_d and λ_d are model parameters.

The parameters of the retention curve of MX-80 bentonite and pellets were determined fitting the experimental data obtained by Eurogeomat (Dang and Robinet, 2004), CIEMAT (Villar, 2003) and Clay Technology (Hökmark and Fälth, 2003) (Fig. 7 and Table 1). As the retention curve depends on the dry density of the materials, the parameters of cylinder, ring, bricks and pellets were determined considering their dry density values (Fig. 7).

For the rest of materials, the original expression proposed by Van Genuchten (1978) was used:

$$S_l = \left[1 + \left(\frac{\psi}{P}\right)^{\frac{1}{1-\lambda}}\right]^{-\lambda} \tag{8}$$

As the permeability for the interface element was adopted higher than for the bentonite, a low value of P was adopted for the
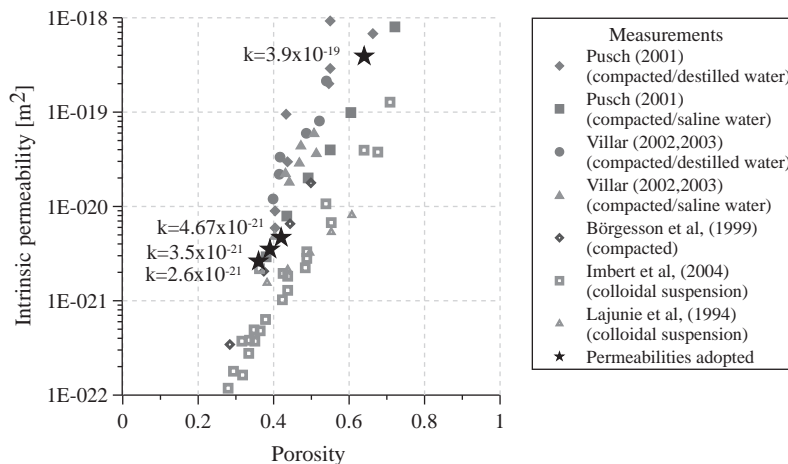

Fig. 6. Variation of intrinsic permeability with porosity for MX-80 bentonite. Experimental results and values adopted.
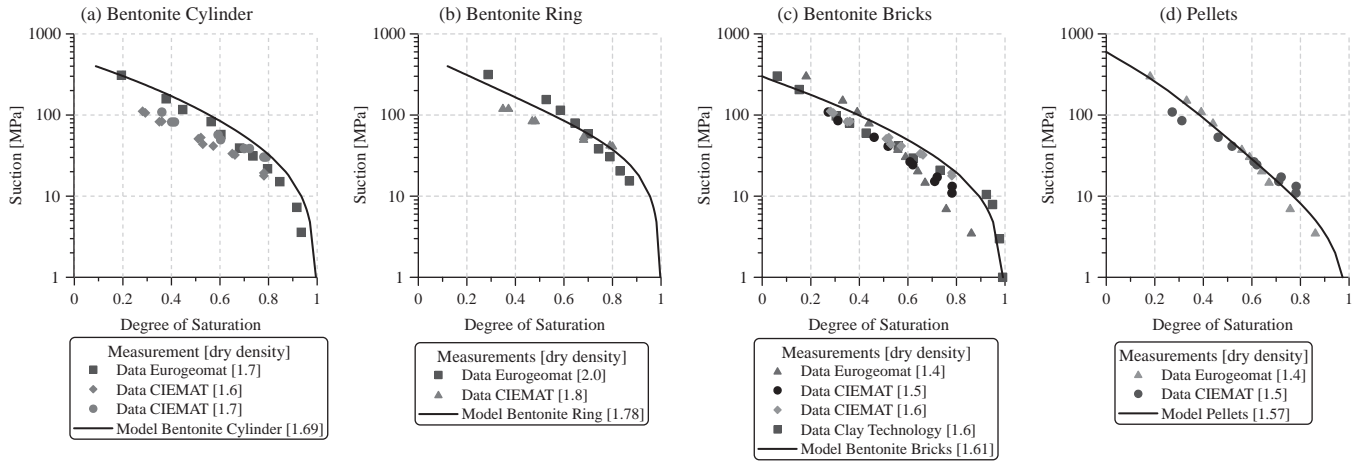
Fig. 7. Retention curves adopted for bentonite cylinder, ring, bricks and pellets in the numerical model and experimental data obtained for different dry densities of MX-80 bentonite. Data provided by Eurogeomat were found in Dang and Robinet (2004), by Clay Technology in Hökmark and Fälth (2003) and by CIEMAT in Villar (2003).

interface element in order to allow a fast drying of those elements (see Fig. 8). The values used for canister, concrete and steel lid did not affect the hydraulic behaviour of the model. As the numerical formulation considered porous medium it is necessary to assume these values to run the analyses.

The hydraulic parameters of the materials are summarised in Table 1.

The vapour diffusion is calculated using Fick's law:

$$D_g^{vapour} = \tau D^v \left[\frac{(273.15 + T)^{2.3}}{P_g} \right] \quad (9)$$

where τ is the tortuosity coefficient. A tortuosity $\tau = 0.8$ is adopted for bentonite; $\tau = 0.9$ for pellets and $\tau = 1.0$ for the interface. The coefficient of diffusion, D^v, is 5.9×10^{-6} m^2/s/K.

5.3. Mechanical properties

5.3.1. Continuum elements

The mechanical constitutive model adopted for MX-80 bentonite and pellets is a modified form of the Barcelona Basic Model; BBM (Alonso et al., 1990). The total strain of the model is calculated adding elastic and viscoplastic strains. The original elastic formulation of BBM is modified to reproduce the expansive behaviour of the bentonite. The elastic model adopted here is:

$$\dot{\varepsilon}_v^e = \frac{\kappa_i(\psi)}{1+e} \frac{\dot{p}'}{p'} + \frac{\kappa_s(p')}{1+e} \frac{\dot{\psi}}{\psi + p_{at}} \quad \dot{\varepsilon}_s^e = \frac{\dot{J}}{G} \quad (10)$$
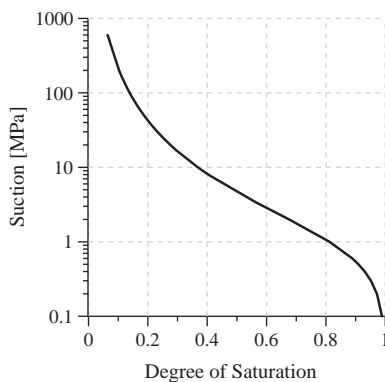

Fig. 8. Retention curve adopted for the interface between canister and bentonite ring.

where ε_v^e and ε_s^e are the volumetric and deviatoric components of the elastic strain respectively; κ_i and κ_s are the elastic stiffness for changes in net mean stress and suction respectively; p' is the mean net stress; ψ is the suction; e is the void ratio, J is the square root of the second invariant of deviatoric stress tensor ($J = \frac{1}{2} trace(\mathbf{s} : \mathbf{s}) = \frac{1}{3} q^2$; $\mathbf{s} = \sigma' - p'\mathbf{I}$); G is the shear modulus.

The elastic stiffness for net mean stress depends on suction as:

$$\kappa_i(\psi) = \kappa_{i0}(1 + \alpha_i \psi) \quad (11)$$

where κ_{i0} is the elastic stiffness in saturated conditions and α_i is a model parameter.

The elastic stiffness for suction depends on net mean stress as:

$$\kappa_s(p') = \kappa_{s0} \left[1 + \alpha_{sp} \ln \left(\frac{p'}{p_{ref}} \right) \right] \quad (12)$$

where κ_{s0} and α_{sp} are model parameters; and p_{ref} is the pressure reference.

The viscoplastic strains ($\dot{\varepsilon}^{vp}$) are calculated as:

$$\dot{\varepsilon}^{vp} = \Gamma \langle \Phi(F) \rangle \frac{\partial G}{\partial \sigma'}; \quad \Phi(F) = \left(\frac{F}{F_0} \right)^N \quad (13)$$

where γ is the viscosity; N is the power of stress; F_0 is a value of reference; F is the yield surface and G is the viscoplastic potential.

The yield surface is defined by:

$$F = 3J^2 - M^2(p' + p_s)(p_0 - p') = 0 \quad (14)$$

And the viscoplastic potential by:

$$G = 3J^2 - \alpha M^2(p' + p_s)(p_0 - p') = 0 \quad (15)$$

where M is the slope of the critical state; p_0 is the apparent unsaturated preconsolidation pressure; p_s considers de dependency of shear strength with suction and α is a model parameter that makes the model non-associated.

The apparent unsaturated preconsolidation (p_0), the variation of compressibility ($\lambda(\psi)$) with suction and the hardening law were calculated according the expression proposed by Alonso et al. (1990).

The elastic stiffness κ_{i0} and α_i; and the parameters of compressibility $\lambda(0)$ r and β for MX-80 bentonite were determined fitting the experimental data obtained by Tang (2005) and Villar (2005) (see Fig. 9). The other parameters were determined from back calculation. The parameters for the pellets were determined based on experimental values obtained by Hoffman et al. (2007).
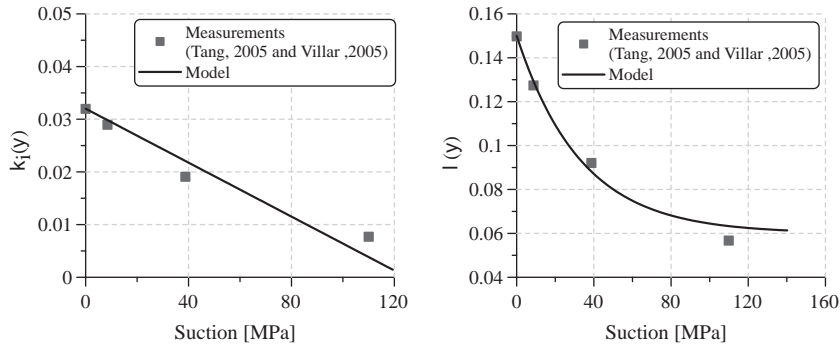
Fig. 9. (a) Variation of MX-80 bentonite elastic stiffness with suction. (b) Variation of compressibility with suction (Tang, 2005; Villar, 2005).

5.3.2. Interface elements

The mechanical behaviour of the interface elements is defined by the relationship between stress and relative displacements in the mid-plane of the interface element (Fig. 10). The stress tensor of the mid-plane is calculated by:

$$\sigma'_{mp} = \begin{bmatrix} \sigma' \\ \tau \end{bmatrix}_{mp} = \mathbf{D}\mathbf{w}_{mp} \tag{16}$$

where σ'_{mp} is the net effective stress of the mid-plane of the element and it is defined as $\sigma'_{mp} = \sigma_{mp} - \max\{P_g; Pl_{mp}\}$; ($mp$ is the total mean stress of the mid-plane; σ is total mean stress; P_g is the gas pressure and Pl_{mp} is the liquid pressure in the mid-plane of the element); τ is the tangential stress of the mid-plane; $\mathbf{D}$ is the stiffness matrix which relate the stress relative displacements with the stress state (see Fig. 10a and b).

The mid-plane relative displacements are interpolated using the nodal displacements and the shape functions (Segura, 2008).

$$\mathbf{w}_{mp} = \begin{bmatrix} u_n \\ u_s \end{bmatrix}_{mp} = \mathbf{r}\mathbf{N}^u_{mp}[-\mathbf{I}_4 \quad \mathbf{I}_4]\mathbf{u}_e \tag{17}$$

where u_n and u_s are the normal and tangential relative displacements of the mid-plane of the element (see Fig. 11b), $\mathbf{r}$ is the rotation matrix that transforms the relative displacements in the local orthogonal coordinate system to the global coordinate system. $\mathbf{N}^u_{mp}$ is a matrix of shape functions, $\mathbf{I}_4$ is a identity matrix of 4th order and u_e is the vector of the nodes element displacement.

The stiffness matrix of the interface relates the normal effective (σ') and the tangential stresses (τ) with the normal (u_n) and the tangential (u_s) displacement of the interface element using normal (K_n) and tangential stiffnesses (K_s), respectively. The normal stiffness depends on the opening of the interface as shown in Eq. (21) (Gens et al., 1990) (see Fig. 10c).

$$\begin{Bmatrix} \sigma' \\ \tau \end{Bmatrix} = \begin{bmatrix} K_n & 0 \\ 0 & K_s \end{bmatrix} \begin{Bmatrix} u_n \\ u_s \end{Bmatrix} \quad K_n = \frac{m}{a - a_{\min}} \tag{18}$$

where m is a parameter of the model; a is the opening of the element and $a_{\min}$ is the minimum opening of the element (at this opening the element is considered closed).

A linear elastic behaviour was assumed for canister, concrete plug and steel lid and their parameters were given in Börgesson (2007).

The mechanical parameters are listed in Table 1.

6. Test observations and model results

In this section test observations (Goudarzi et al., 2006) are compared with the predictions of the numerical analysis.

6.1. Thermal

The temperature at MX-80 bentonite barrier and host rock wall is recorded by Thermocouple sensors. The evolutions of temperature at Cylinder 3, Ring 5 and Ring 10 are shown in Fig. 11a and the temperatures on the host rock wall are plotted in Fig. 11b. The analysis reproduces the observations quite well. The agreement of temperatures indicates that the values of the thermal conductivities of the materials, particularly in the interface, are well captured.

6.2. Hydraulic

Fig. 12a–c shows the variation with time of relative humidity measured by capacitive sensors. The relative humidity from the numerical simulation is calculated using Kelvińs equation:

$$RH = \exp\left[\frac{\psi M_w}{R(273 + T)\rho_l}\right] \tag{19}$$

where ψ is the total suction; M_w is the molecular weight of water; R is the ideal gas constant, T is the temperature and ρ_l is the liquid density.

In the cooler section of the barrier (Cylinder 3) and in the bentonite close to the host rock wall (sensors W137, W142, W119 and W120) a monotonic increase of relative humidity is recorded. This is due to the condensation of the vapour coming from the heated
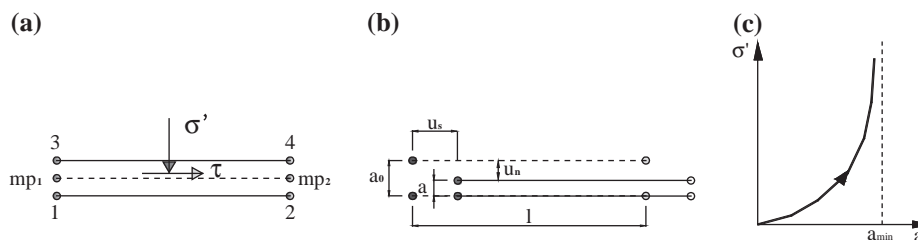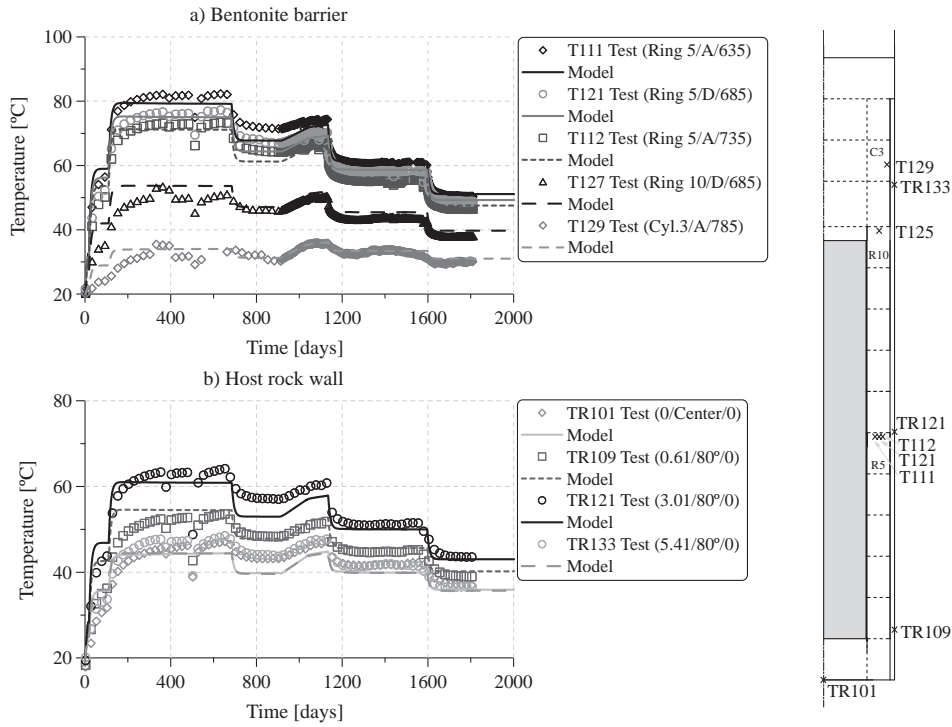

Fig. 10. Interface element with double nodes. (a) Stress state at the mid-plane of the interface element. (b) Relative displacement defined at mid-plane. (c) Elastic constitutive law of interface elements. Normal stiffness depends on interface opening.

Fig. 11. Evolution of temperatures in the bentonite barrier and on the host rock wall. Measured data and model results.
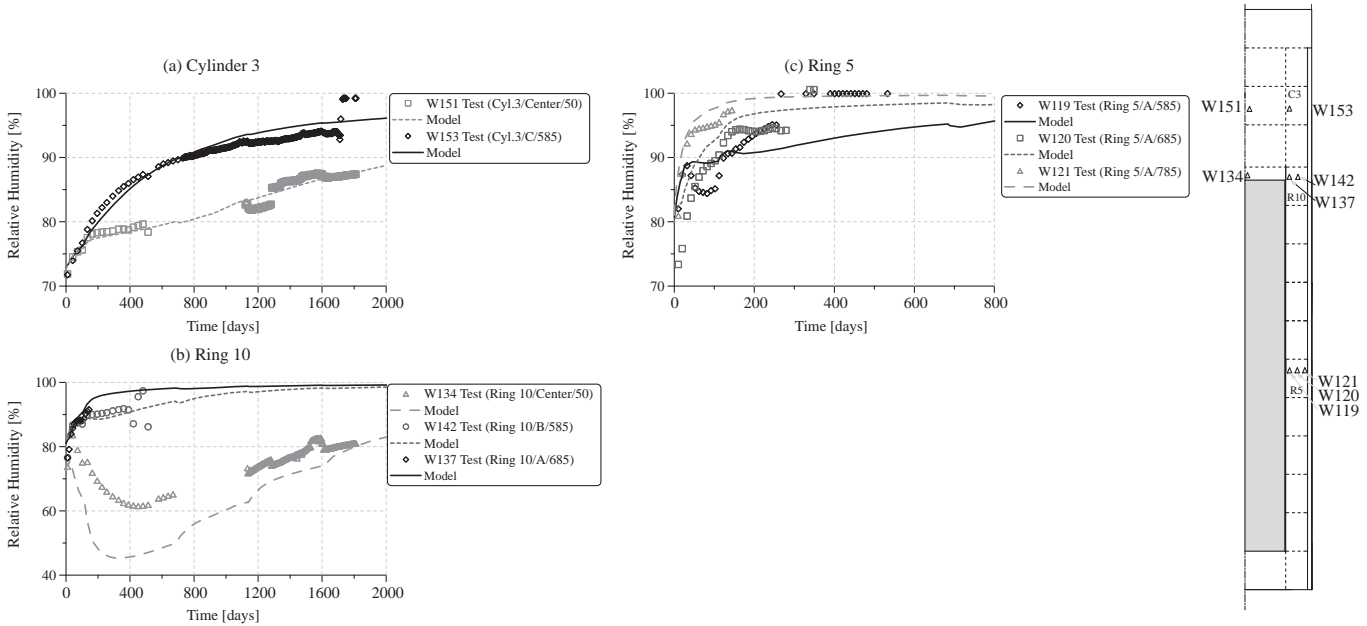

Fig. 12. Evolution of relative humidity in bentonite barrier. (a) Cylinder 3, (b) Ring 10, and (c) Ring 5. Test observations and numerical results.

zones, to the water inflow from the rock and to the artificial hydration from filter mats (Fig. 12a).

However the bentonite barrier closer to the canister exhibits an increase of relative humidity due to the vapour front driven by heating. Then the barrier dries because of the evaporation caused by the increment of the temperature. And finally, the barrier hydrates and its relative humidity increases due to the water inflow from the filter mats and rock (sensor W134 – Ring 10) (Fig. 12b). Nevertheless, at Ring 5, the drying is followed by a fast increment of relative humidity. This may be attributed to the

presence of water in the interface (see Fig. 12c – sensor W119). This water is in form of vapour and hydrates the barrier. In general, the predictions from the numerical model are quite satisfactory.

The evolutions of suction measured with psychrometers and the calculated values are plotted in Fig. 13. There is not a good match between experimental and calculated results; however the decreasing trend of suction with the increment of water content of the buffer is predicted. The suction calculated decreased throughout the test; in contrast, the suctions measured kept
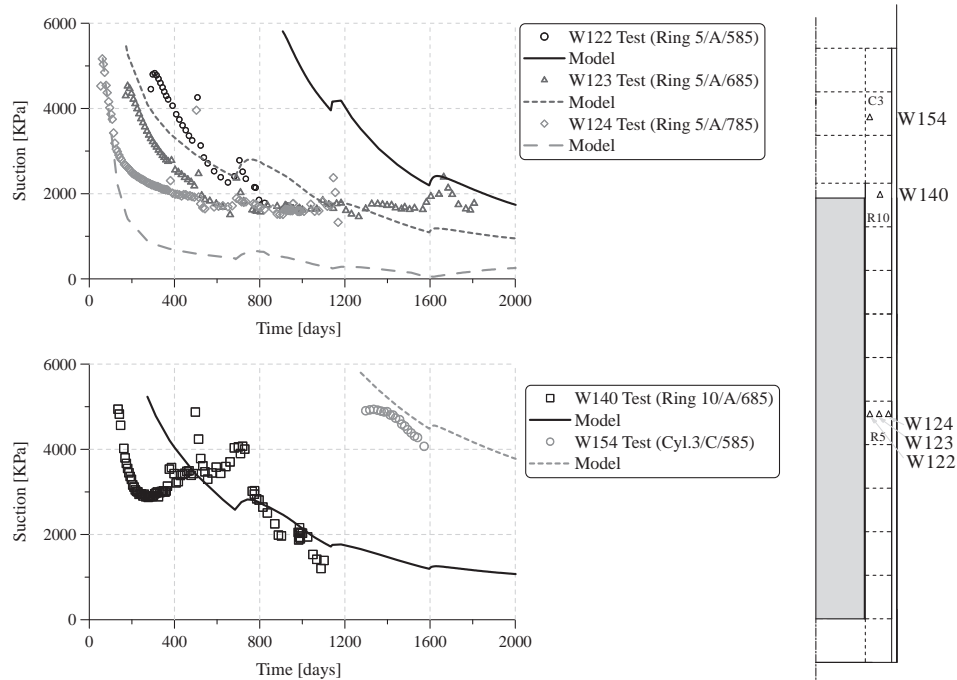
Fig. 13. Evolution of suction in bentonite barrier Ring 5, Ring 10 and Cylinder 3. Test observations and numerical results.
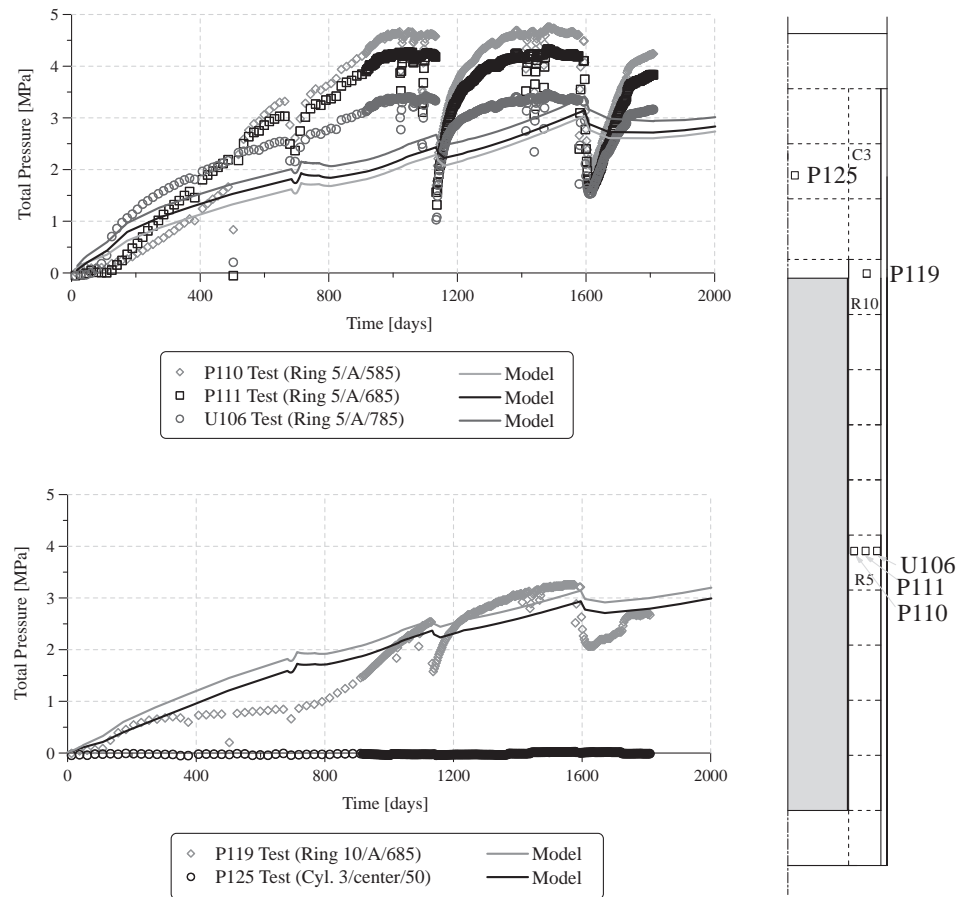

Fig. 14. Evolution of total pressure in the bentonite barrier. Experimental data and numerical results.

constant at 2 MPa from day 800 up to the test end, perhaps due to osmotic effects not considered in the analysis. Considering osmotic effects would require the incorporation of chemical variables in the formulation (Gens, 2010).
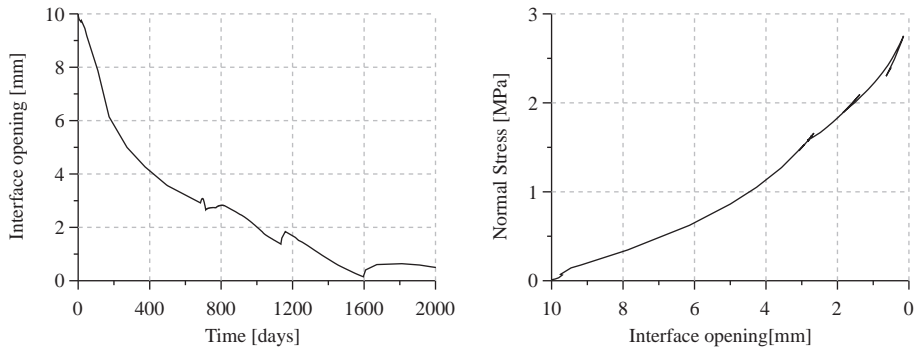
Fig. 15. Evolution of opening and normal stress of the interface between canister and bentonite barrier.

6.3. Mechanical

The total vertical pressure (vertical stress) for the bentonite barrier is plotted in Fig. 14. The swelling of bentonite causes stress increases up to 3.0–4.5 MPa. The numerical results underestimated the magnitude of the stresses but follow their trend. The results could probably be improved would improve using a mechanical model that considers the double structure of expansive clays (Sánchez and Gens, 2006).

In Fig. 15 the evolutions of the opening and of the normal stress of the interface are shown. The interface closes and its stress increases as the bentonite swells. The final opening of the slot is approximately 2 mm and the maximum normal stress is 2.5 MPa corresponding to the stress calculated in the bentonite barrier next to the slot (Fig. 14 – radial distance 585 mm).

7. Test dismantling

After test dismantling, samples at selected sections were cored from bentonite and pellets. In Cylinder 3, samples were extracted from depths 50, 150, 250, 350 and 450 mm measured from the top of the block. In Ring 10, samples were extracted at depths of 50, 110 and 175 mm. At Ring 6, samples were taken from a depth of 50 mm and directions α = 45°, 135°, 225°, 315° (see Fig. 2). The dry density and water content of samples were measured in the laboratory and the corresponding degree of saturation was calculated (Johannesson, 2007). The values of degree of saturation and dry density for (a) Cylinder 3, (b) Ring 10, and (c) Ring 6 are shown in Fig. 16.

In the figures, the final degree of saturation throughout the bentonite barrier is higher than the initial one even in the zone close to the canister. The degree of saturation is higher near the host rock wall, as a consequence of natural and artificial hydration.

The figures also show that the dry density of bentonite blocks (Cylinder and Rings) decreases due to their swelling. As the swelling of bentonite depends on its hydration, the dry density of the bentonite decreases more in the zones located near the borehole wall. However, the dry density of bentonite bricks increased because they did not swell much due to their low degree of hydration and compressed when the bentonite rings swelled. Also the bentonite swelling caused the compaction of pellets and, consequently, an increase of their dry density.
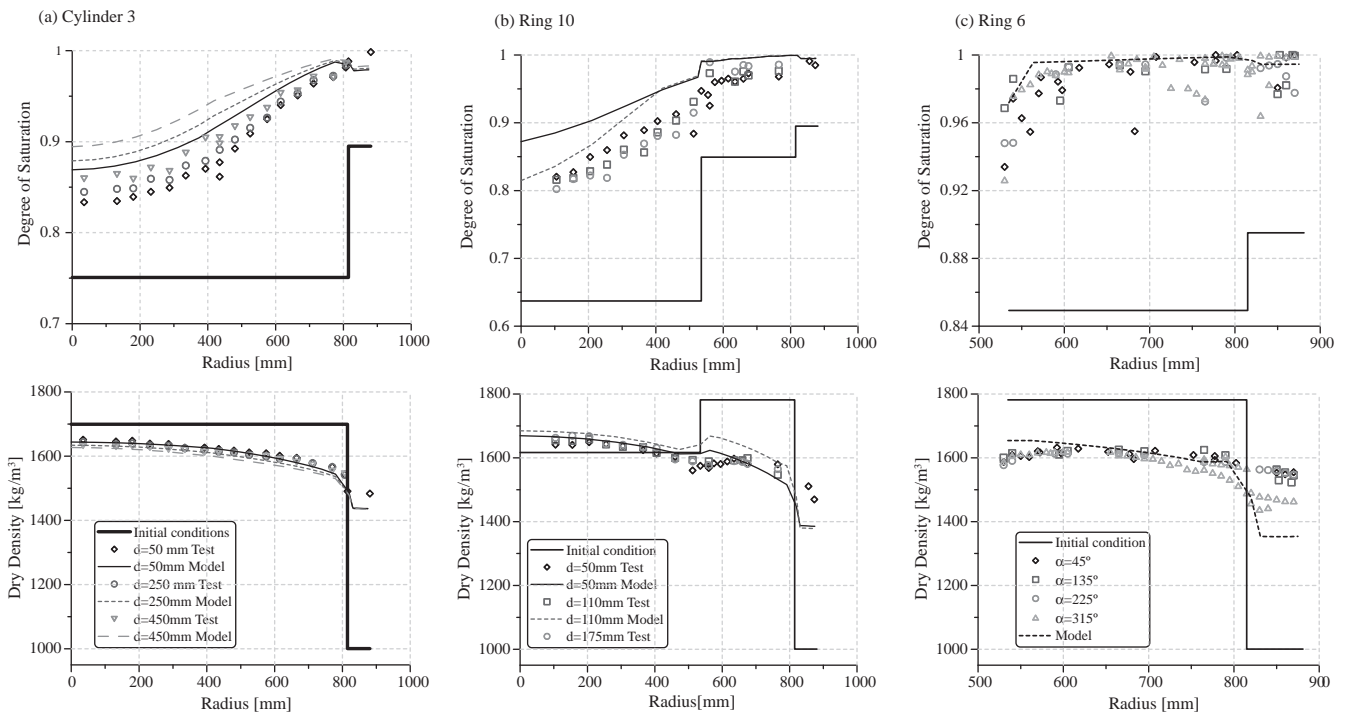

Fig. 16. Degree of saturation and dry density of Cylinder 3, Ring 10 and Ring 6 after test dismantling. Experimental and model results.

8. Conclusions

A coupled THM numerical simulation of borehole disposal scheme for nuclear waste has been performed satisfactorily. The required material parameters have been mostly determined using data from laboratory tests; others were estimated from back analysis.

To model the interface between canister and bentonite a specific mechanical formulation of this element was implemented in Code-Bright. The mechanical formulation is expressed at the mid-plane of the element and relates the relative displacements of the mid-plane with the normal and tangential stress through normal and shear stiffness respectively. In particular, a normal stiffness dependent on interface opening allows the capture of non-linear behaviour under normal stress. Hydraulic and thermal behaviour were modelled in accordance with Darcýs and Ficḱs laws, respectively. The parameters of the interface were fitted by back calculation.

The comparison of the results measured in situ with the results of numerical analysis shows that the formulation used is able to reproduce satisfactorily the phenomena involved in the test as well as their interactions. Moreover, the model has been able to capture the final state of the bentonite and pellets showing the high degree of homogenisation of their dry density achieved during the test. Nevertheless, the magnitude of suction and total stresses would improve incorporating chemical effects in the formulation and adopting a mechanical model which considered the double structure of expansive clays.

Also, it has been possible to verify from the results that the model implemented for interfaces is able to simulate satisfactorily interface behaviour. The evolution of its opening and stress development is mainly controlled by the progress of bentonite swelling.

References

Alonso, E.E., Gens, A., Josa, A., 1990. A constitutive model for partially saturated soils. Geotechnique 40 (3), 405–430.

Börgesson, L., 2007. Canister Retrieval Test, Compilation Made for the EBS Task Force.

Börgesson, L., Hernelind, J., 1999. Coupled Thermo-Hydro-Mechanical Calculations of the Water Saturation Phase of a KBS-3 Deposition Hole, Technical Report TR-99-41.

Börgesson, L., Johannesson, L.-E., Sandén, T., Hernelind, J., 1995. Modelling of the Physical Behaviour of Water Saturated Clay Barriers. Laboratory Tests, Material Models and Finite Element Application, SKB Technical Report 95-20.

Börgesson, L., Johannesson, L.-E., 1995. Thermo-Hydro-Mechanical Modelling of Water Unsaturated Buffer Material, SKB Work Report 95-32.

Börgesson, L., Fredrikson, A., Johannesson, L.-E., 1994. Heat Conductivity of Buffer Materials, SKB Technical Report 94-29.

Dang, K.D., Robinet, J.-C., 2004. Thermo-Hydro-Mechanical Behaviour of MX80 Bentonite for Temperature ⩾100 °C. Final Report. ANDRA Report C.RP.0EUG.02.008.

Gens, A., 2010. Soil-environment interactions in geotechnical engineering. 47th Rankine Lecture. Geotechnique 60 (1), 3–74.

Gens, A., Carol, I., Alonso, E.E., 1990. A constitutive model for rock joints; formulation and numerical implementation. Comput. Geotech. 9, 3–20.

Goudarzi, R., Börgesson, L., Röshoff, K., Edelman, M., 2006. Sensors Data Report (Period: 001026-060501) Canister Retrieval Test, Report No. 12.

Hoffman, C., Alonso, E.E., Romero, E., 2007. Hydro-mechanical behaviour of bentonite pellet mixtures. Phys. Chem. Earth 32, 832–849.

Hökmark, H., Fälth, B., 2003. Temperature Buffer Test. Predictive Modelling Programme. Äspö Hard Rock Laboratory Internal Report F12.1G 1012125.

Imbert, C., Billaud, P., Touze, G., Dang, K.D., 2004. Comportement thermo-hydro-mécanique d'une argile gonflante méthodologique en situation de stockage. CEA, Rapport RT-DPC/SCCME 04-677-A.

Johannesson, L.E., 2007. Dismantling and sampling of the buffer and determination of density and water ratio. International Progress Report IPR-07-16, SKB, Stockholm, Sweden.

Lajudie, A., Raynal, J., Petit, J.-C., Toulhoat, P., 1994. Clay based materials for engineered barriers. A review. Mater. Res. Soc. Symp. Proc. 353, 221–230.

Pintado, X., Ledesma, A., Lloret, A., 2002. Backanalysis of thermohydraulic bentonite properties from laboratory tests. Eng. Geol. 64 (2–3), 91–115.

Pusch, R., 2001. Experimental Study of the Effect of High Porewater Salinity on the Physical Properties of a Natural Smectitic Clay. SKB Tech. Rep. TR 01-07.

Sánchez, M., Gens, A., 2006. FEBEX Project: Final Report on Thermo-Hydro-Mechanical Modelling, Technical Publication 05-2/2006. Madrid. Enresa.

Sánchez, M., 2004. Thermo-Hydro-Mechanical Coupled Analysis in Low Permeability Media. Ph.D. Thesis, Universitat Politècnica de Catalunya (UPC), Barcelona. 281 pp.

Segura, J. Ma., 2008. Coupled HM Analysis using Zero-Thickness Interface Elements with Double Nodes. Tesis de Doctorado-Universidad Politécnica de Catalunya, Barcelona.

Sugita, Y., Chijimatsu, M., Suzuki, H., 2003. Fundamental Properties of Bentonite Pellet for Prototype Repository Project, Advances in Understanding Engineered Clay Barriers, Large Scale Field Tests in Granite: Fundamental Research. Material Behaviour and Laboratory Testing, pp. 293–301.

Tang, A.M., 2005. Effect de la temperature sur le comportement des barrieres de confinement. PhD Thesis, CERMES, ENPC, Paris, France.

Thorsager, P., Börgesson, L., Johannesson, L.-E., Sandén, T., 2002. Canister Retrieval Test, Report on Installation, International Progress Report 02-30.

Van Genuchten, M. Th., 1978. Calculating the Unsaturated Hydraulic Conductivity with a New Closes Form Analytical Model. Research Report 78-WR-08. Dept. of Civil Eng., Pricenton, New Jersey, p. 63.

Villar, M.V., 2002. Thermo-Hydro-Mechanical Characterisation of a Bentonite from Cabo de Gata. A Study Applied to the Use of Bentonite as Sealing Material in High Level Radioactive Waste Repositories. Publicación Técnica ENRESA 01/2002, Madrid. 258 pp.

Villar, M.-V., 2003. "AESPOE Hard Rock Laboratory". CIEMAT Contribution to 2001 Annual Scientific Report. CIEMAT Internal Report CIEMAT/DIAE/54540/2/03.

Villar, M.V., 2005. MX-80 Bentonite, Thermo-Hydro-Mechanical Characterisation Performed at CIEMAT in the Context of the Prototype Project, CIEMAT Technical Report, Madrid, Spain.